2015

USE OF LIDAR-DERIVED TERRAIN AND VEGETATION INFORMATION IN A DECIDUOUS FOREST IN KENTUCKY

Wesley A. Staats
University of Kentucky, wast223@uky.edu

STUDENT AGREEMENT:

I represent that my thesis or dissertation and abstract are my original work. Proper attribution has been given to all outside sources. I understand that I am solely responsible for obtaining any needed copyright permissions. I have obtained needed written permission statement(s) from the owner(s) of each third-party copyrighted matter to be included in my work, allowing electronic distribution (if such use is not permitted by the fair use doctrine) which will be submitted to UKnowledge as Additional File.

I hereby grant to The University of Kentucky and its agents the irrevocable, non-exclusive, and royalty-free license to archive and make accessible my work in whole or in part in all forms of media, now or hereafter known. I agree that the document mentioned above may be made available immediately for worldwide access unless an embargo applies.

I retain all other ownership rights to the copyright of my work. I also retain the right to use in future works (such as articles or books) all or part of my work. I understand that I am free to register the copyright to my work.

REVIEW, APPROVAL AND ACCEPTANCE

The document mentioned above has been reviewed and accepted by the student's advisor, on behalf of the advisory committee, and by the Director of Graduate Studies (DGS), on behalf of the program; we verify that this is the final, approved version of the student's thesis including all changes required by the advisory committee. The undersigned agree to abide by the statements above.

Wesley A. Staats, Student

Dr. Marco A. Contreras, Major Professor

Dr. David B. Wagner, Director of Graduate Studies

USE OF LIDAR-DERIVED TERRAIN AND VEGETATION INFORMATION IN A DECIDUOUS FOREST IN KENTUCKY

THESIS

A thesis submitted in partial fulfillment of the
requirements for the degree of Master of Science in the
College of Agriculture, Food, and the Environment
at the University of Kentucky

By

Wesley Staats

Lexington, Kentucky

Director: Dr. Marco A. Contreras, Assistant Professor of Forest Management

Lexington, Kentucky

2015

ABSTRACT OF THESIS

USE OF LIDAR-DERIVED TERRAIN AND VEGETATION INFORMATION IN A DECIDUOUS FOREST IN KENTUCKY

The use of Light Detection and Ranging (LiDAR) information is gaining popularity, however its use has been limited in deciduous forests. This thesis describes two studies using LiDAR data in an Eastern Kentucky deciduous forest. The first study quantifies vertical error of LiDAR derived digital elevation models (DEMs) which describe the forests terrain. The study uses a new method which eliminates Global Positioning System (GPS) error. The study found that slope and slope variability both significantly affect DEM error and should be taken in to account when using LiDAR derived DEMs. The second study uses LiDAR derived forest vegetation and terrain metrics to predict terrestrial Plethodontid salamander abundance across the forest. This study used night time visual encounter surveys coupled with zero-inflation modeling to predict salamander abundance based on environmental covariates. We focused on two salamander species, *Plethodon glutinosus* and *Plethodon kentucki*. Our methods produced two different best fit models for the two species. *Plethodon glutinosus* included vegetation height standard deviation and water flow accumulation covariates, while *Plethodon kentucki* included only canopy cover as a covariate. These methods are applicable to many different species and can be very useful for focusing management efforts and understanding species distributions across the landscape.

KEYWORDS: Light Detection and Ranging, Digital Elevation Model, Salamander, Zero-inflated model, Visual Encounter Survey

Wesley A. Staats

August 1, 2015

USE OF LIDAR-DERIVED TERRAIN AND VEGETATION INFORMATION IN A DECIDUOUS FOREST IN KENTUCKY

By

Wesley Staats

Dr. Marco A. Contreras
Director of thesis

Dr. David B. Wagner
Director of Graduate Studies

August 1, 2015
Date

AKNOWLEDGEMENTS

I would like to thank many people for their help and involvement in the construction of my thesis. First, my major professor, Dr. Marco Contreras, and my advising comittee members, Dr. Steven Price, and Dr. Christopher Barton for their advice and guidance. I would like to thank David Parrott for his hard work, advice, moral support, and friendship. I would also like to thank my fellow lab members, Suraj Upadhaya, Mark Lin, and Sandhya Nepal for their encouragemnt, support, and friendship. Additionall I would like to thank Dr. John Lhotka, Dr. James Ringe, Dr. Mary Arthur, and Rob Paratley for providing additional advice, experice and encouragement. I would also like to thank the Director of Graduate Studies, Dr. David Wagner, for always being available for advice and for his quick responses to emails. My fellow classmates have been extremely encouraging and supportive and I would like to thank them as well. Finally, I would like to thank Chris Osborne and the Robinson Forest staff for their help with field work and for providing many replacement vehicles for transportation within Robinson Forest.

Table of Contents

List of Figures

List of Tables

Chapter 1: Background on Light Detection and Ranging and its Use in Forestry and Natural Resource Conservation

Light detection and ranging (LiDAR) technology

Light detection and ranging (LiDAR) technology has been used since the 1970's, originally developed for terrestrial military purposes and atmospheric particle mapping (Carter et al., 2012). However, in the past 15 years, LiDAR has made great advancements and gained popularity in the commercial sector (Reutebuch et al., 2005). LiDAR information is collected by using a laser range finder to scan surfaces' position in space. The system is made up of a laser emitter, laser receiver, highly accurate timing device and an onboard computer. The LiDAR system is able to measure the distance to an object by illuminating a surface with a laser beam pulse of near-infrared light. The receiver intercepts reflected photons and a computer calculates the distance to the surface based on the time it takes the light to travel there and back. Then, given a known position of the LiDAR system, an accurate position of the surface can be calculated. The LiDAR system pulses the laser beam at a rate of 10,000 -100,000 pulses per second in order to quickly collect many position readings for an object or surface. The diameter of the beam is often between 0.2 m and 1m which allows for some photons to pass behind smaller objects and reflect off of further objects. In this way, LiDAR can measure up to 5 point positions per beam pulse. The data collected from a LiDAR system can be received either in discrete point positions of surfaces or in a wave form that displays the frequency of photons collected by the receiver for the entire duration of time that the beam is moving. It is possible to extract more instances of the beam contacting a surface from wave form data because even

small fluctuations in photon returns are recorded that might not be interpreted as a discrete point position (Reutebuch et al., 2005).

Airborne LiDAR systems are able to quickly gather information over large areas. To maintain accurate measurements in an airborne LiDAR system, dual frequency 2 Hz GPS receivers coupled with an inertial measurement unit are used to track the exact location of the plane. A laser scanner system capable of 10,000 to 100,000 pulses second^{-1} is used to calculate the distances to measured surfaces (ASPRS LiDAR Committee, 2004). All discrete points measured from a single beam pulse are assigned a location based on the single average trajectory of the beam. Therefore wider beams will result in less accurate measurements, while beam width is larger the further the plane is from the ground (Reutebuch et al., 2005). Typically Airborne LiDAR can yield vertical root mean squared errors of 10-15 cm and 15-100 horizontal root mean squared errors (Reutebuch et al. 2003).

The usefulness of LiDAR data is also dependent on the density and evenness of spacing of the point data. The density of points is affected by the height of the plain above the ground and the frequency of beam pulses the LiDAR system emits. For a given system pulse frequency, point density can be increased by flying lower to the ground. However, the lower the plane flies to the ground, a plane will have to make a greater number of passes over an area to cover it entirely because the reach of the beam will be reduced (Reutebuch et al., 2005). There may also be legal restrictions on how low an airplane can fly in an area. There are different scanning systems that can pulse their beams at different frequencies and in different patterns, higher

frequency systems generally costing more. Thus there is a trade off in cost between flying height affecting the cost of collecting the data and the initial cost of selecting a transmitter.

The different types of beam patterns have different costs and benefits associated with them as well. The ideal beam pattern would be evenly homogeneously spaced points and beams aimed perpendicular to the ground. However this is practically impossible to achieve. The most common system uses a single emitter that adjusts the angle of its beam to cause a zig-zag pattern across the ground. This pattern is not homogenous, points will be closer to each other at the edge of the reach of the scanner and the edge beam pulses will have a large scan angle. The scan angle is the deviation from a true perpendicular line to the ground, meaning the larger the scan angle the further the beam has to travel to hit the ground. This could lead to more error by allowing the beam width to expand and allowing the beam a greater chance to be intercepted by objects before it reaches the ground. To counter this, pilots will fly the plane so that the flight paths overlap by approximately 20% (Reutebuch et al., 2005). Then a portion of the points in those overlapping edges are removed to create a more homogeneous pattern. (Lefsky et al, 2002). There are also oscillating beam scanners that scan a circular beam pattern, so the points are more evenly spaced than a zig-zag pattern but the scan angle is still an issue. There are also sensors that shoot multiple beams at the same time, which are parallel to one another. This type of scanner can have high pulse frequencies and avoids the high scan angle problem, but the flight path does not have a wide reach so a plane needs to make more passes to cover the same area and the initial cost of having more scanners is higher than the other options. In general a more dense LiDAR data distribution will cost much more than less dense data (Lefsky et al, 2002).

LiDAR data and primary processing

LiDAR systems typically record many different attributes for each LiDAR point datum. They include: XYZ coordinates, point ID, intensity, return number, number of returns per pulse, classification code, GPS time, scan angle, scan direction flags, and whether the point is on the edge of the flight line. Some more recent scanners can even record RGB color reflectance. Originally the data was stored in the ASCII text format, however now with higher point density and larger operations the industry has moved to the Log ASCII Standard (LAS) file format which can store the same information in a smaller file (ESRI, 2014). An LAS file is a binary file that contains header information followed by individual point information which can also be compressed in an even smaller LAZ file format. The most commonly used attributes are the XYZ coordinates, intensity, and return number (the order that the points were assigned from a single beam pulse). In the wave form data the first peak of photons returned in a single beam pulse would be considered the first return. This would be the highest object that a beam hit and would be the first photons to return to the receiver. The number of returns per beam can be affected by the width of the beam and the size of the objects the photons are hitting. The scan angle can be used in the point filtering process to improve the overall accuracy and homogeneity of the data collected (Sangster, 2002).

After the initial information is collected the data is processed by filtering out redundant point from overlapping flight paths, and points considered to be noise. Noise points can be caused by ambient reflected photons or photons reflected off of unintended objects such as flying birds, insects, or low dense clouds. Noise points are often either located lower than previously known terrain or much higher than other points. It is important to note that higher

density LiDAR data needs much more computing space and power to store, and more processing than low density data, so the filtering step is very important to make all other processing easier (Sangster, 2002). The data is further processed by classifying each point by surface type. The most basic surface types are ground points and non-ground points. However, common point classifications include ground, low vegetation, medium vegetation, high vegetation, building, water, and noise.

The points are classified by using either commercial software, e.g, TerraScan, or using one's own software or algorithms. There are a few different traits that ground points are assumed to have that aid software developers in identifying ground points. Ground points are usually located lowest in the data, so it is common to start by selecting the lowest points in a neighborhood window. It is also assumed that the slope between ground points on a surface are lower than the slope between other objects. So surfaces that have high slopes compared to the general known terrain will often be removed. It is also assumed that bare ground generally has few sharp differences in elevation, so those points that deviate greatly in elevation from the rest will be removed (Meng et al., 2010).

There are several procedures that are commonly practiced, often in combination, to identify ground points based on the aforementioned traits. The first most basic and most common process is to remove outliers, which are points that are either extremely high or extremely low. They can come from birds, insects, other airplanes or ambient noise. This is done by examining elevation distributions and removing points that deviate greatly from the mean (Meng et al., 2010). Another very popular procedure developed by Kraus and Pfeifer

(1998) is linear prediction. This method also uses statistical processes to assign weights to points based on their position to a rough estimate of the surface between ground and no ground points. This process is repeated using points with negative residuals by moving the estimated surface closer and closer to the true ground (Liu, 2008). This method is not very accurate in areas with steep slopes and high terrain variability because it assumes a relatively smooth, flat ground surface. Another method developed by Vosselman, (2000) is based on the assumption that ground points will have a relatively low slope in relation to each other. This method is most successful at differentiating between ground points and other objects such as trees and buildings. This is done by setting a threshold of acceptable slopes within a given circular window. The threshold is adjusted based on known terrain slopes, and becomes less accurate as terrain slopes increase (Liu, 2008). This method can be improved by adjusting the threshold with previously known rough slope and terrain information (Sithole, 2001). Finally a progressive morphological filter can be used by converting the LiDAR points to a greyscale raster image based on elevation and removing non ground objects based on the difference in grey tone in a certain window (Liu, 2008). The progressive aspect comes from modifying the procedure using fixed window sizes to use variable window sizes that gradually get larger to remove both small objects such as trees and large objects such as building roofs from the ground points (Zhang et al., 2003). This method is performed assuming a flat slope, however Chen et al. (2007) proposed a similar method that adjusts for terrain slope assuming that changes in elevation between the ground and objects will be abrupt but changes in elevation due to terrain will be gradual. Once ground points are identified the remaining points can be

further classified in to groups including low, medium, and high vegetation, buildings, water, and noise (ESRI, 2014).

After points are classified, digital elevation models (DEM), or three–dimensional representations of terrain, can be created. The three most common ways to represent a DEM are to assign a constant elevation value to pixels in a square grid, use a triangular irregular network (TIN) to represent elevation, and displaying changes in elevation with contour lines (Liu, 2008). The simplest and most common form is the square grid and we will be referring to this form henceforth when discussing DEMs. The value of each cell is assigned by interpolating values between neighboring LiDAR points.

There are several different interpolation methods for creating such a model. The inverse distance weighting method assigns a value to a cell by weighting each LiDAR point based on its distance to the center of the cell. Therefore points located closer to the center of the cell will be more influential on the cell's value (Anderson et al., 2005). This method assumes even distribution of LiDAR points and does not produce accurate results when data is sparse or uneven (Childs, 2004). This method also cannot produce values outside the minimum and maximum sample point values and is less useful when representing ridges or valleys (Lee, 2004). The spline method uses a mathematical equation, like a regression, that represents a sheet draped over the ground points, passing directly though the points. This method produces a smooth portrayal of the surface and is able to produce values outside the minimum and maximum point values. This method is best for terrain with valleys and ridges that aren't represented well in the point data (Childs, 2004). The kriging method fits a function to points

within a search window based on a spatial correlation of those points. This method can also exceed the range of sample values but the surface generated does not necessarily have to pass directly through the point data. High density data provides best results for this model, producing a less smooth model than spline, and can also be more accurate in rough terrain (Liu, 2008). Natural Neighbor is another weighted average method similar to IDM but works well with clustered and uneven points and very large datasets (Childs, 2004). There is software available such as ArcMap that can easily create the different types of DEMs using these varied methods.

DEMs created from LiDAR data are used in city planning, flight planning, transportation, agriculture, natural resource conservation and forestry. DEMs can be further manipulated using common geographic information system (GIS) software such as ArcMap to estimate slope, aspect, shaded relief (hillshade), curvature, water flow accumulation, watershed delineation, and many other parameters (ESRI, 2014). There are also many other uses for LiDAR data outside of creating DEMS. LiDAR non-ground vegetation point data are a very useful in the forestry and natural resource fields. The data can be used to estimate tree locations, tree density, diameter at breast height (DBH), tree heights, crown widths, canopy cover, individual tree species (Kim, 2008), light transmittance, volume, and biomass. The Majority of these parameters can be estimated based on a digital surface model (DSM). This model is similar to a DEM however while a DEM is a representation of the lowest LiDAR points, a DSM is a representation of the highest LiDAR points. In a forested area the tops of trees are usually the highest points in a landscape and therefor the DSM represents the elevation of treetops. A DSM can be made with similar processes to DEMs while just using either the maximum points in a

window or an interpolation of the first returned points. The DSM raster can then be subtracted from a DEM raster and the yielding vegetation height model (VHM). The VHM is processed further to produce many of the parameters mentioned above (Goerndt, 2011).

LiDAR-derived individual tree detection

The majority of individual tree based methods for estimating individual tree locations use an algorithm called variable window filtering which uses variable sized search windows to find local maximum point clusters. These clusters are assumed to be the peak of the tree crown and the width of the search window is assumed to be the crown width. The methods usually also use a DEM to calculate tree height ,then use algometric equations based on tree species and height to estimate the diameter at breast height, volume, or biomass. This method usually requires a very uniform forest structure with coniferous species and a fairly high density LiDAR Data. The conical shape of conifer crowns make the local maxima searches more accurate (Wannasiri et al, 2013; Popescu, 2007). Koch et al. (2006) uses a crown delineation process that starts with a smoothed VHM to avoid over estimating tree density, locating peaks in a similar fashion as mentioned above, then from those peeks expands the crown width until slope reverses or the crown meets another tree's crown. Once crowns are delineated crown width can easily be extracted and tree height can be estimated by extracting the maximum height value within the crown. Then DBH and volume can be estimated using algometric equations based on species, with tree height and crown width as variables (Heurich, 2008; Dalponte et al., 2011).

While it is much easier to estimate DBH and volume in uniform coniferous stands a study by Wannasiri et al (2013) used two methods to estimate individual tree biomass parameters for mangrove trees. The first method was a variable window filter method while the second method was an inverse watershed method to find tree peek locations. The inverse watershed method is performed similarly to how hydrologists delineate watersheds and locate flow outputs. A DSM of the canopy is made and inverted so that the tops of the trees would be the lowest points. Then the watersheds are delineated by creating a flow accumulation raster where the top of the tree would have the highest flow accumulation and the edges of the crown would have the lowest flow accumulation. Then tree height and crown width were used to calculate DBH and biomass from algometric equations specific to mangrove trees. This study is notable because mangrove trees have round shaped crowns rather than conical shaped crown found in conifers, and could be used in other hardwood forests. They found that the variable window filter was slightly more accurate when compared with ground measurements. Another similar forest measurements study was done by Rahman and Gorte (2008) attempted to locate trees without a uniform shape. They used a combination of inverse watershed method and point densities to locate tree centers, assuming that the center of a tree would contain the most points in a vertical column. This method is more promising than the variable width filter method because it doesn't base its window size on tree height therefor can be done for trees with different crown to tree height relationships and is promising for use in hardwood forests.

LiDAR-derived stand level information

Currently assessments of individual trees through use of LiDAR data is most accurately performed for homogenous coniferous forests with high density LiDAR data (Koch et, al., 2006). However if the data is sparse or the structure of the individual trees are not uniform, then a stand level approach that generalizes the data over a larger area is more practical and more precise (Popescu, 2007). Bater et al (2009) assessed using LiDAR to quantify standing dead tree class distributions in a hemlock forest. They used a stand based approach with a high resolution (0.5m) VHM to calculate point vegetation height mean, maximum standard deviation and coefficient of variation for each cell and regressed them to data collected in the field. They found that the coefficient of variation was the best predictor variable for vegetation structure and used that to extrapolate to the rest of the forest. Vogeler et al (2013) performed a similar study quantifying vegetation in another western conifer forest in order to predict a forest health indicating bird species' (*Certhia americana*) presence. They found that the density of the upper canopy was the most predictive variable and were able to adequately predict the presence of the brown creeper at monitored sites.

Other LiDAR applications in natural resources

LiDAR data is very versatile and has many uses in natural resource fields. LiDAR derived DEMs are particularly useful because of their high vertical accuracy in forested areas (Liu, 2008). DEMs are are also used widely in hydrological studies. Because DEMs are a 3D representation of the ground, they can easily be used to predict water movement. Hydrologists often need to estimate catchment size and delineate watersheds when managing water resources. This previously required going out to the field and using surveying equipment which

is time intensive and expensive. Now there are common programs such as ArcGIS that can delineate watersheds quickly and accurate solely from a DEM.

There have been many studies that show that fine resolution of DEM aren't necessary for accurate watershed parameters (Charrier and Li, 2012; Yang et al, 2014). Thus, less expensive lower density LiDAR derived DEMs can be used to estimate water parameters and have become more cost effective than field measurements. One study showed that low vegetation interference in LiDAR ground data caused inaccuracy when delineating watershed boundaries with a high resolution DEM (Goulden et al, 2014). Another study demonstrated how a DEM can be used to calculate stream outflow points to delineate watersheds when previously field hydrometric stations were used to locate outflow points (Lindsay et al, 2008).

The algorithms behind delineating watershed boundaries involve using a DEM to calculate slope and aspect of cells of a raster which are then used to calculate the direction water would flow. The result is a raster called a flow accumulation which estimates for each cell how many cells above it would theoretically drain water into that cell (Matsunaga at al, 2009). This information is useful in hydrology calculations such as calculating stream locations and lengths because the cells with the highest flow accumulation value should be located in a stream. There have also been studies that show that DEM resolution doesn't need to be high in order to estimate accurate stream locations and lengths. High resolution DEMs have been shown to increase then estimated length of the streams (Goulden et al, 2014). This is more evidence that less expensive LiDAR data can be adequate in some situations.

Information from DEMs can also be used to estimate relative soil moisture and forest productivity in an area. Because soil moisture is largely dependent on terrain information such as slope, aspect, and curvature, DEMs can be used to model an integrated soil moisture index which has many forestry and natural resource applications. Iverson et al (1997) used a combination of flow accumulation, curvature and hillshade (an estimation of direct sunlight reaching a slope) derived from a DEM combined with USDA soil water holing capacity data to estimate an integrated moisture index for their study area. Then they compare it with known site indices of species in the area to make a predictive map of site index and species composition.

Chapter 2: Quantifying Error in Variously Interpolated DEMs from a Complex Deciduous Forest with Varying Slopes and Terrain Features

Introduction

Airborne light detection and ranging (LiDAR) data are invaluable for natural resource applications due to its quick and accurate data collection over large landscapes. The data measure coordinate point positions of objects and terrain by using high frequency laser rangefinder technology. LiDAR data are often used to model surface terrain features to create a Digital Elevation Model (DEM). LiDAR derived DEMs require vastly less time and effort than traditional ground surveying of large landscapes. Another alternative to ground surveying is photogrammetry which uses multiple aerial images of a landscape to calculate depth and topographic relief. LiDAR is more accurate and cost effective than photogrammetry in areas with vegetation cover such and forests, and areas that have low relief and low texture such as wetlands and costal dunes (Lefsky et al, 2002). While low density LiDAR data contain accurate point data the resulting DEM would also be of low resolution. The use of high point density LiDAR data is becoming more popular, as it allows for interpolating higher resolution DEMs. Studies have shown that the resolution of a DEM is a very important factor when calculating terrain derivatives such as slope and curvature (Kienzle, 2004) and using higher resolution DEMs when delineating flood boundaries result in more accurate predictions of flooding hazards (Alho et al., 2009). Understanding how LiDAR derived DEM accuracy is affected by different landscape conditions is an important area of research.

There are many different factors to take in to account when evaluating the accuracy of LiDAR derived DEMS. The characteristics of the measuring instruments and flight path of the

plane can affect the accuracy of the raw data points (Liu, 2008; Stereńczak, and Kozak, 2011) while the point filtering (Sangster, 2002) and interpolation methods (Kraus and Pfeifer, 1998; Liu, 2008; Meng et al., 2010; Sithole, 2001) need to be chosen according the quality of LiDAR data and characteristics of the landscape it is describing. It is commonly recognized that vegetation low to ground decreases LiDAR accuracy by increasing the uncertainty that light reflecting from the ground actually hits the ground (Stereńczak, and Kozak, 2011). However, canopy cover and forest structure can also affect the density and distribution of points representing the ground. Hyyppa et al. (2005) agree that accuracy of DEMs vary as a function of slope, undergrowth and forest cover. They also found that error increases as measurements become closer to the trunk of a tree due to fewer LiDAR data points reaching the ground. DEM accuracy has shown to be very high in coniferous forest, while slightly decreasing as forest cover increases (Reutebuch et al., 2003) and accuracy of DEMs is highest under flat open canopy areas with smooth surfaces (Clark et al., 2004). While many studies quantify error in either coniferous or low vegetation or leaf off conditions (Gould et al., 2013; Hodgson and Bresnahan,2004; Spaete et al.,2011) or low to gently sloped areas (Hodgson et al., 2005; Su and Bork, 2006; Spaete et al.,2011;) studies that quantify error in both densely vegetated and highly sloped areas are rare.

Deciduous forest often have dense, complex canopy structures made up of multiple species leading to less LiDAR penetration, less accurate DEMs, and slower adoption of LiDAR derived DEMs. There has been a lack of research evaluating DEM accuracy in dense forests with a complex forest structure and many species (Stereńczak, and Kozak, 2011) specifically with respect to differences in slope and slope variability or ruggedness. The Appalachian Mountains

of the United States provide an ideal setting to evaluate LiDAR derived DEM accuracy under such conditions. This area is not only similar in vegetation structure and topography to a large portion of the Eastern United States but also to other understudied areas such as South America and East Asia, which could benefit immensely from LiDAR adoption. Quantifying DEM accuracy in mountainous deciduous forest is especially important in North America because of LiDAR's increase in commercial use (Lefsky et al., 2002) and the interest in the availability of large scale state wide and nationwide LiDAR datasets. (Stoker, J., et al., 2007; Farrell, 2012) In the Appalachian Mountains, high resolution DEMs could have many important uses in forest operations, mining operations, and wildlife conservation. Understanding how error varies across different topography in already error prone landscapes is essential before wide scale DEM adoption.

The objectives of this study were 1) quantify DEM error based on slope and ruggedness in a complex deciduous forest, 2) determine whether LiDAR dataset density or interpolation method have an effect on error , and 3) evaluate a new method for quantifying DEM error in areas where global positioning system (GPS) accessibility is limited. We hypothesize that DEM error will increase with increasing slope and ruggedness, and that that high density LiDAR will provide the least error. Traditional methods for quantifying DEM vertical accuracy involves finding the difference between check points measured by an assumed higher accuracy method such as a differential GPS (Aguilar and Mills, 2008). We constructed a study designed to remove the vertical error associated with GPS devices that could be used in areas that provide poor GPS signal, which also provides error values for a whole topographic surface rather than point error measurements. The plot centers are identified within the LiDAR data by their relation to known

nearby terrain features to compare the information for the exact same location in the DEM. Then field data was collected for differences between elevations measurements from the center point to points taken around the plot center and compared to DEM values to provide an error associated with that whole surface. This eliminates the error of GPSs having uncertain vertical accuracy and provides a more useful metric than single point comparisons in ruggedly sloped areas. The setting for this study is University of Kentucky's Robinson Forest, a mixed mesophytic deciduous forest with variable slopes from 2-80 percent located in the Cumberland Plateau region of Kentucky on the southern extent of the Appalachian Mountains. This forest is very representative of the complex forest structure and topography of the rest of the Cumberland Plateau and recent high-density and low-density LiDAR data has been collected for this area presenting a unique opportunity to improve the understanding of DEM accuracy in an understudied landscape.

Methods

Study Area

Research was conducted at The University of Kentucky's Robinson Forest (Lat. 37.4611, Long. -83.1555), located in the rugged eastern section of the Cumberland Plateau region of southeastern Kentucky in Breathitt, Perry and Knott counties (Figure 1). Due to access limitations, we restricted the study area to the Clemons Fork and Lewis Fork watersheds within Robinson Forest. Terrain across the study area and the entire Robinson Forest is characterized by a branching drainage pattern, creating narrow ridges with sandstone and siltstone rock formations, curving valleys and benched slopes. The slopes are dissected with many intermittent streams (Carpenter and Rumsey, 1976) and are moderately steep ranging from 10

to over 100%, predominately northwest and southeast aspects, and elevation ranging from 252 to 503 meters above sea level. The bedrock transitions from sandstone to siltstone, shale and coal heading downslope (Smalley, 1986), with predominant soil types being Cloverlick-Shelocta-Kimper, Matewan-Marrowbone-Latham, Shelocta-Gilpin-Hazleton which are all deep well drained rocky soils silt-loams (Hayes, 1998). The climate of this area is temperate humid-continental with warm summers and cool winters (Overstreet, 1984), with average annual temperature of 12.8 °C, average annual precipitation is 117.5 cm, and average monthly precipitation is 9.76 cm (Cherry 2006). Vegetation is comprised of a diverse contiguous mixed mesophytic forest made up of approximately 80 tree species with northern red oak (*Quercus rubra*), white oak (*Quercus alba*), yellow-poplar (*Liriodendron tulipifera*), American beech (*Fagus grandifolia*), eastern hemlock (*Tsuga canadensis*) and sugar maple (*Acer saccharum*) as dominant and codominant species, while understory species include eastern redbud (*Cercis canadensis*), flowering dogwood (*Cornus florida*), spicebush (*Lindera benzoin*), pawpaw (*Asimina triloba*), umbrella magnolia (*Magnolia tripetala*), and bigleaf magnolia (*Magnolia macrophylla*) (Carpenter and Rumsey, 1976 ; Overstreet, 1984). Average canopy cover across Robinson Forest is about 93% with small openings scattered throughout. Most areas exceed 97% canopy cover but recently harvested areas have an average cover as low as 63%. After being extensively logged in the 1920's, most of Robinson Forest is considered second growth forest ranging from 80-100 years old, and is protected from commercial logging and mining activities that are typical land uses in the region (Overstreet, 1984).

LiDAR Datasets

We used two LiDAR datasets covering the study area, collected with the same LiDAR system by the same vendor. One dataset was low density (~ 1 pt m^{-2}) collected in the spring of 2013 during leaf-off season for the purpose of acquiring terrain information, as a part of a state-wide elevation data acquiring program from the Kentucky Division of Geographic Information (KDGI). The second dataset was high density (~ 40 pt m^{-2}) collected in the summer of 2013 during leaf-on season for the purpose of collecting detailed vegetation information and ordered by the University of Kentucky' Department of Forestry (UKDF). The parameters of the LiDAR system and flight for both datasets are presented in Table 2.1. The vendor processed both raw LiDAR datasets using the TerraScan software (Terrasolid Ltd., 2012) to classify LiDAR points into ground and non-ground points. A third dataset was also created by combining both low-density and high-density points. For each of the three LiDAR datasets (low-density, high-density, and combined), the "Create LAS Dataset" tool in ArcMap 10.2 was used to create a Log ASCII Standard (LAS) dataset file. The LAS dataset was then filtered to include ground points only, and the "LAS dataset to Raster" tool in ArcMap was used to create a 1-meter resolution DEM using the natural neighbor as a fill void method. Four DEMs for each dataset were created considering different interpolation methods: average, inverse distance weighted, minimum, and nearest neighbor. As a result, a total of 12 DEMs covering the study area were created; three LiDAR datasets and four interpolation methods.

Sampling Design

We expected that LiDAR-derived DEM errors will vary with terrain steepness and ruggedness. As these terrain features are typically calculated for each cell using the elevation

values from the eight adjacent cells, the 1-m resolution of the LiDAR-derived DEM is too fine and will likely capture micro-terrain variations. For the purpose of identifying different levels of terrain steepness and ruggedness, we calculated the slope raster and resampled it to a coarser resolution of 36.6 m (120 ft.) using the average value. This resolution was selected to provide a more meaningful scale for the study area and to match the size of field plots used to collect terrain surface information. The coarse resolution slope raster was used to identify terrain steepness across the study area and to create three slope classes (low, medium, and high) containing the same relative area (Figure 2.2a, Table 2.2). Terrain ruggedness at the same coarse 36.6 m resolution was calculated as the slope variability of the 1-m slope raster, as used by Ruszkiczay-Rudiger et al. (2009) to determine slope heterogeneity, thus ruggedness. Slope variability for each cell in the coarse resolution raster was defined as the range (max slope – min slope) of slope values in the 1-m resolution slope raster (Figure 2.2b). The study area was then divided into three slope variability classes (low, medium, and high) with the same relative area (Table 2.2). The slope and slope variability raster layers were then overlaid to identify the nine combined slope/ruggedness classes. Five field plots were randomly located in each combined classes resulting in a total of 45 field plots (Figure 2.3).

Field Plot Data Collection

The general location of the 45 field plots were determined using a hand-help GPS unit. Triangulation from easily identifiable features in both the LiDAR-derived raster layers and on the field were used to refine field plot locations with sub-meter accuracy. These features consisted of trees, rock formations, road intersection, and other road features (i.e., cut and fill slope areas, ditch relief culverts, and bends). Once the location of a given plot was identified,

eight transects extending 18.3 m (60 ft.) from plot center were established covering 360° at 45° intervals (four cardinal and four ordinal directions). At six points along each transect, every 3.05 m (10 ft) of horizontal distance from plot center, we measured elevation change (vertical distance) between the points and the plot center (Figure 2.4). Transect directions and elevation change of points along transects were measured using an electronic compass (MapStar Compass Module II, Laser Technology Inc.) and a sighted laser range finder (Impulse 200 LR, , Laser Technology Inc.). Elevation change for the 48 points (8 transect × 6 points) were measured by mounting the electronic compass and laser range finder on a tripod at the plot center, and moving a target mounted on a pole at the same height above the ground as the range finder to each points. A given point location was deemed acceptable when horizontal distance from the laser range finder and the target was within 0.06 m and azimuth within 1^{o}

Data Analysis

The x- and y-coordinates of the 2,160 points (45 plots × 48 points) were obtained based on the coordinates of the corresponding plot center, and the horizontal distance from plot center and azimuth of the corresponding transect. For a given point, the LiDAR-derived DEM elevation change was obtained from the elevation values of the DEM cells containing the point location and the plot center location. Elevation changes from the field plots were considered true values and LiDAR-derived elevation errors were obtained by calculating the absolute difference between field plot elevation changes from DEM-derived elevation changes. The total 2,160 elevation errors were arranged by plot number, and combination of slope and ruggedness class. Elevation changes were obtained from the 12 different DEMs and mean

elevation errors were calculated by slope and ruggedness class to examine the effect of the LiDAR dataset and interpolation method.

Additionally, we expected that elevation errors would increase with horizontal distance from plot center due to field difficulties to correctly measure distances (horizontal and vertical) using laser range finder caused by abundant understory vegetation. Therefore, we formally tested for significant differences in the mean elevation error among slope and ruggedness categories as well as distance from plot center using a 3-way ANOVA in SAS 9.3 (Statistical Analysis Software, SAS Institute, Cary, NC, USA).

Results

When combining DEM-derived elevation changes from all three LiDAR datasets and four interpolation methods, the resulting mean elevation error was about 73.6 cm (Table 2.3). Mean elevation errors among LiDAR datasets were similar within 1.5 cm, while the high-density and combined datasets providing the lowest and highest errors, 72.7 cm and 74.1 cm respectively. No significant differences were found among LiDAR datasets, as evidence by 95% confidence intervals (Figure 2.5). When comparing interpolation methods, mean elevation errors were even more similar with values ranging from 73.4 – 73.8 cm (Figure 2.5).

As expected mean elevation errors increased with slope and ruggedness level (Figure 2.6). Mean elevation errors ranged between 42.0 – 101.2 cm from low to high slope classes, and between 63.2 – 92.7 cm from low to high ruggedness classes. Although mean elevation errors among slope and ruggedness classes are significantly different, due to non-overlapping 95% confidence intervals, slope seems to have a larger effect as evidenced by the larger variation. Even more variability in mean elevation errors can be observed when considering

individual combinations of slope and ruggedness, ranging from 23.2 – 145.5 cm for the low slope and low ruggedness and high slope and high ruggedness, respectively (Figure 2.7). Within the high ruggedness class, there is a clear increase in mean elevation error with increasing slope with all classes being significantly different. Although in the other two ruggedness classes the mean elevation errors generally increases with slope, there is a less clear pattern. Within the medium ruggedness class, the high slope class has the highest error which is significantly different that the medium and low slope classes. Within the low ruggedness class, the low slope class has a significantly different and lowest mean elevation error.

When averaging elevation errors by distance from the plot center, there was a clear increase in error as distance from the plot center increased. The lowest mean elevation error of 34 cm was found for the points 3.0 m from the plot center and increased almost linearly to the highest of 111.6 cm for measurements taken at points 18.3 m from plot center (Figure 2.8). A three-way ANOVA that combined elevation errors from all LiDAR datasets and interpolation methods corroborate previous results. Differences of mean elevation errors among slope classes ($Pr F<0.0001$), ruggedness classes ($Pr F < 0.0001$), and distance from plot center ($Pr F <0.0001$) were all significantly different. We also found a significant interaction between slope and ruggedness ($Pr F <0.0001$). There was no significant interactions between ruggedness and distance, slope and distance, or ruggedness and slope and distance ($Pr F >0.05$). In addition, slope classes had the highest F-Value of three effects tested, which is further evidence that slope has a greater impact on elevation error. Ruggedness and distance had similar effects, but the effect of ruggedness was slightly larger.

Seeing as error increased as distance from the plot center increased we ran the analysis again considering only the 3.0 m from the plot center field measurements. The overall mean elevation error decreased to 34.1 cm, which is about 46% of the mean using all measurements. Again, there were no significant differences between LiDAR dataset and interpolation method (Figure 2.9). The same increasing mean elevation error with slope level was observed, with averages by slope class being significantly different and ranging from 19.3 to 44.5 cm (Figure 2.10). Although the same pattern can be observed for ruggedness level, the mean elevation errors of the medium and high classes are 3.0 cm apart and significantly different, and the mean elevations error for the low ruggedness class is significantly lower than the medium and high classes (Figure 10). When examining mean elevation errors by slope and ruggedness combinations we also observed larger variations of 14.5 cm for the low ruggedness /low slope class to 56.2 cm for the high ruggedness /medium slope class (Figure 2.11). Within the high ruggedness class, the mean elevation error for the high slope class was slightly smaller than that for the medium slope class (50.6 and 52.6 cm) but they were statistically similar, as evidenced by the overlapping 95% confidence intervals there were no significant differences. The mean elevation error for the low slope class was much smaller, 17.7 cm and statistically different. Mean elevation error also increased with increasing slope level within the medium ruggedness class, with values ranging from 25.6 – 56.2 cm. Within the low ruggedness class, the mean elevation error is lowest for the low slope class, which significantly different than the medium and high classes. Results from a two-way ANOVA using only measurements taken 3.0 m from plot center also showed significant slope ($p<0.0001$) and ruggedness effects ($p<0.0001$) on the mean elevation error (Table 2.5). There is also a significant interaction between slope

and ruggedness ($p<0.0001$) and F-values also show that slope is the most significant source of error.

Discussion

In this study, we used a different approach to quantify elevation error of LiDAR-derived DEMs in areas where GPS readings are not reliable due to limited signals from terrain steepness and a dense forest canopy. Thus, instead of determining the elevation ground points using GPS units, we determined plot center locations from reference features within LiDAR data and quantified relative elevation changes from plot center ground points to multiple adjacent points within 18.3 m horizontal distance. This approach was more appropriate to assess the ability of LiDAR-derived DEMs to accurately represent terrain surfaces. The overall mean elevation error from the surface terrain represented by the LiDAR-derived DEMs was about 74 cm, which is much higher than the standard 15 cm accuracy quoted for most LiDAR systems (Baltsavias, 1999). This is likely because standard accuracies are reported for ideal conditions with flat ground and no vegetation cover.

Although our overall mean elevation error is within values reported in the literature, 0.1 – 2.7 m (Edson and Wing, 2015), it is higher than errors provided by several studies. A likely reason is the concentric design of points within each field plot used to collect elevation change. The horizontal threshold used to establish point locations (± °1 azimuth and ± 0.06 m of horizontal distance) inherently increases horizontal error with distance from plot center, and in steep terrain a slight horizontal error can create a significant elevation error (Flood, 2004). This elevation error is increased in rugged terrain with numerous rock formations. What is more, the further away from plot center the more likely the laser range finder is to intercept small

vegetation (i.e., stray branches, twigs, leaves, or vines) which could interfere with the reported vertical distances. However, when considering measurement taken 3.0 m from plot center, mean elevation errors are comparable with those reported by other studies(Edson and Wing, 2015).

Our results showed that both slope and ruggedness had a significant effect on the mean elevation error. This is likely due to the misclassification of LiDAR points into ground and non-ground (vegetation) points. Classification algorithms assume that the lowest elevation LiDAR point in a given window (1×1 m) is a ground point and that slope between adjacent ground points is lower than slope between ground points and adjacent non-ground. In steep and rugged terrain, these assumptions typically result in ground points with higher elevations than the lowest elevation point within the given window being misclassified as low vegetation (Meng et al., 2010). This misclassification of LiDAR points are likely numerous in areas with small rock formations (i.e., outcrops and cliffs) and slopes steep enough that tree crowns are in close proximity to the ground, such as that of our study area. An example of such misclassification can be seen in figure 2.12, which results in underestimation of DEM elevation values and thus increased elevation errors.

Although large differences in point density of our LiDAR datasets are present, there were no statistical differences in mean elevation error among LiDAR datasets. A possible reason is that the high-density dataset was collected during the leaf-on season and only a small proportion of points were able to penetrate the canopy and reach the ground level. This is especially true for areas under large, dense tree crowns. In the case of the low-density dataset, as it was collected during the leaf-off season, more points were able to reach the ground and

thus point spacing was more even. Figure 2.13 illustrates the spatial distribution of ground points of the three LiDAR datasets where only a small amount of additional ground points can be observed in the high-density dataset. In addition gaps caused by dense tree crown can be clearly identified. The similar quality of surface elevations observed between the low- and high-density datasets is an important result from our study because it indicates no need to invest additional resources into more expensive denser datasets if the data can be collected during leaf off. Therefore, managers and practitioner interested in using LiDAR-derived DEMs to accurately represent terrain surfaces and elevations can acquire low-density dataset unless also interested in obtaining vegetation metrics.

Our results showed no significant differences among interpolation methods with variation in mean elevation error of 1 cm. The main reason is the relatively fine resolution of the LiDAR-derived DEM. Other studies evaluating different interpolation methods have found significant differences for larger resolution and similar result for fine resolutions (Arun, 2013; Setiyoko and Kumar, 2012). As aforementioned, these four interpolation method are commonly used by LiDAR data vendors to create DEMs and based on our results the selection of interpolation does not affect elevation quality. Lastly, future research should focus evaluating the elevation accuracy of LiDAR derived DEM, specifically in complex terrain and vegetation condition of mountainous deciduous forests of the central Appalachia.

Research evaluating classification algorithms to separate ground points from non-ground points is needed to identify appropriate methods that reduce the misclassification of ground points on rugged terrain as low vegetation and vice versa, thus improving elevation accuracy. Moreover, Li et al. (2011) showed an example of smoothing efforts in a prairie region

of Canada. Similar efforts could be used to smooth over depressions caused by LiDAR point voids near dense deciduous tree. Lastly, additional efforts can focus on optimizing raster cell size in order to minimize effects ground point voids.

Conclusion

Our method for evaluating DEM accuracy proved useful and was most successful at quantifying elevation error when limiting field measurements to 3m from plot center, providing errors in the lowest slope and ruggedness classes, similar to other studies. Under the dense vegetation and steep topographic conditions of our study site we found that DEM accuracy is dependent on both slope and ruggedness, as expected, with slope having a greater effect on error. The direct causes of the error are most likely due to misclassification of ground points as vegetation, which is worsened as slope increases. We encourage researches and managers to try and account for this increased DEM error for practices such as stream delineation and wetland identification where elevation accuracy is crucial. DEMS are often the starting point of many analyses and require several transformations to derive useful information, therefor any DEM error would be magnified in the final result. Our main suggestion to ensure accurate DEMs is to research LiDAR data providers to find one with experience in forested areas so that their algorithms are more accurate at quantifying ground points when dense vegetation is present. It is also best to collect your LiDAR data in the winter when the absence of leaves will create fewer voids in the data. As we found no difference in DEM errors between high and low density LiDAR datasets it might be more financially optimal to purchase a lower density dataset that uses a more advanced sensor that could provide more accurate values for each point. Our suggestions will improve DEM accuracy but not eliminate all of the error caused by high slope

and ruggedness. In order to achieve this, more research needs to be conducted to find more effective was to classify ground points and interpolate data with large voids.

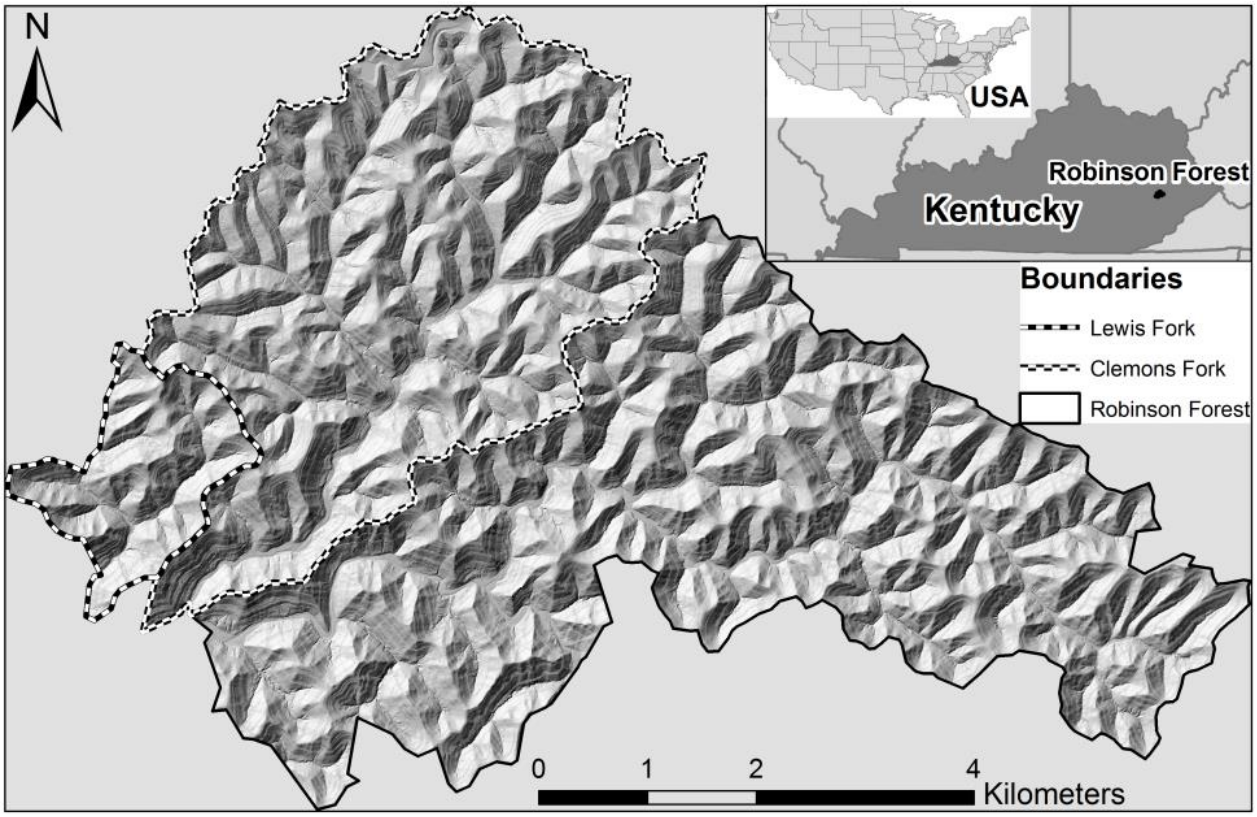

Figure 2.1. Topography of the study area (1,797 ha) within Robinson Forest (4,250 ha) located in Breathitt, Knott, and Perry counties in southeastern Kentucky (Lat. 37.4611, Long. -83.1555).

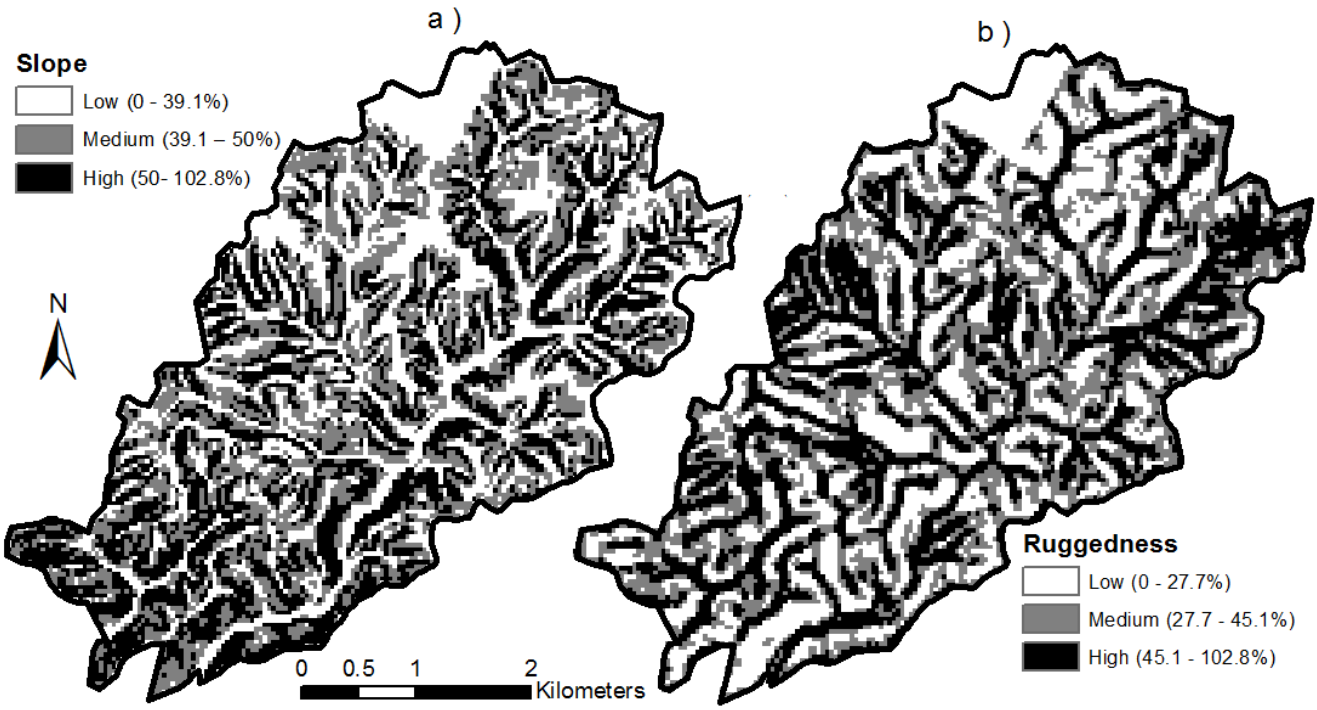

Figure 2.2. Coarse, 36.6 m resolution raster layers showing percent slope (a) and variability of percent slope variability, terrain ruggedness (b) across the study area used to create the nine combinations of slope/ruggedness categories.

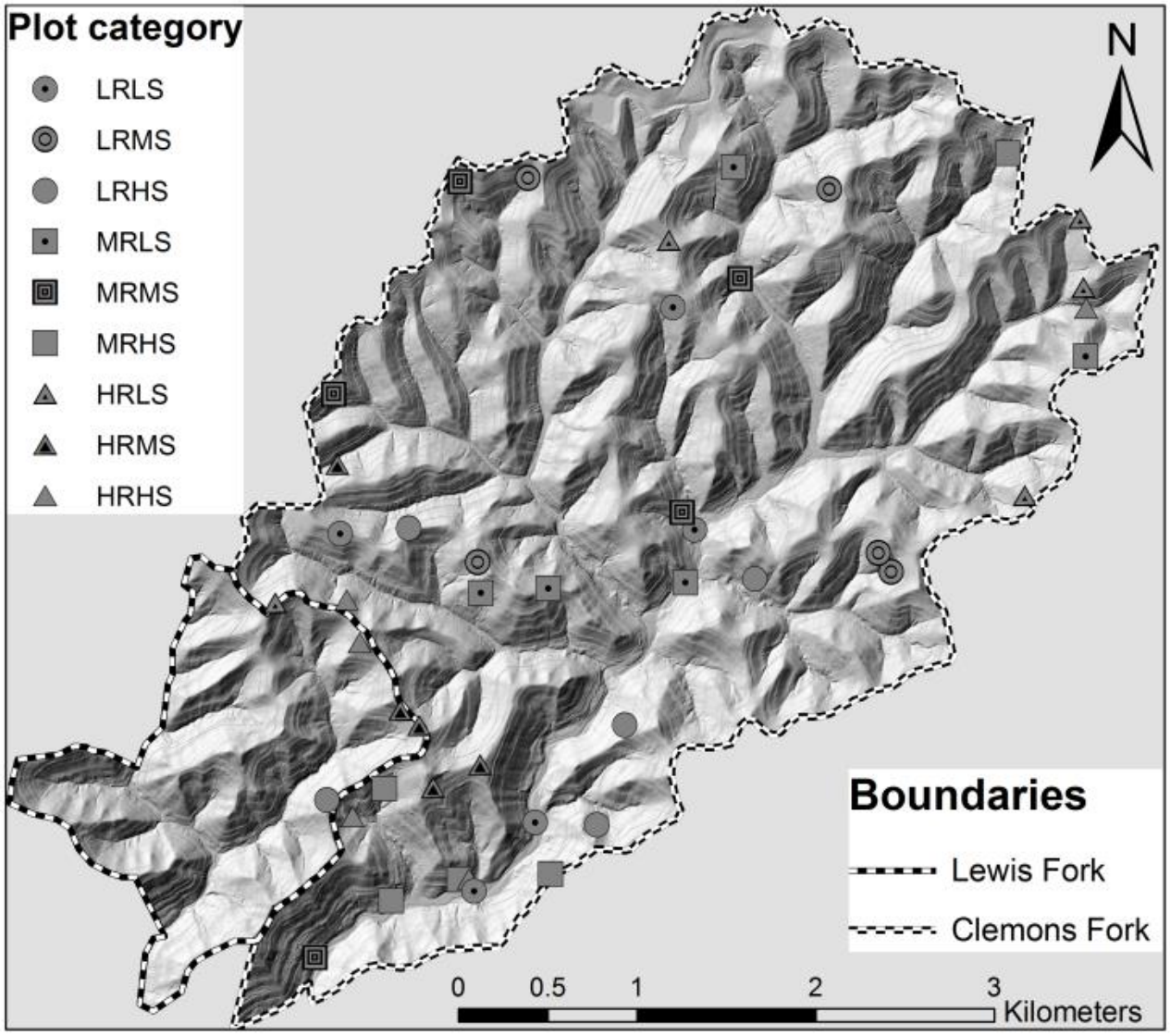

Figure 2.3. Location of field plots within the study area. First letter in the abbreviated plot categories indicates level of ruggedness (second letter) and third letter indicates level of slope (fourth letter).

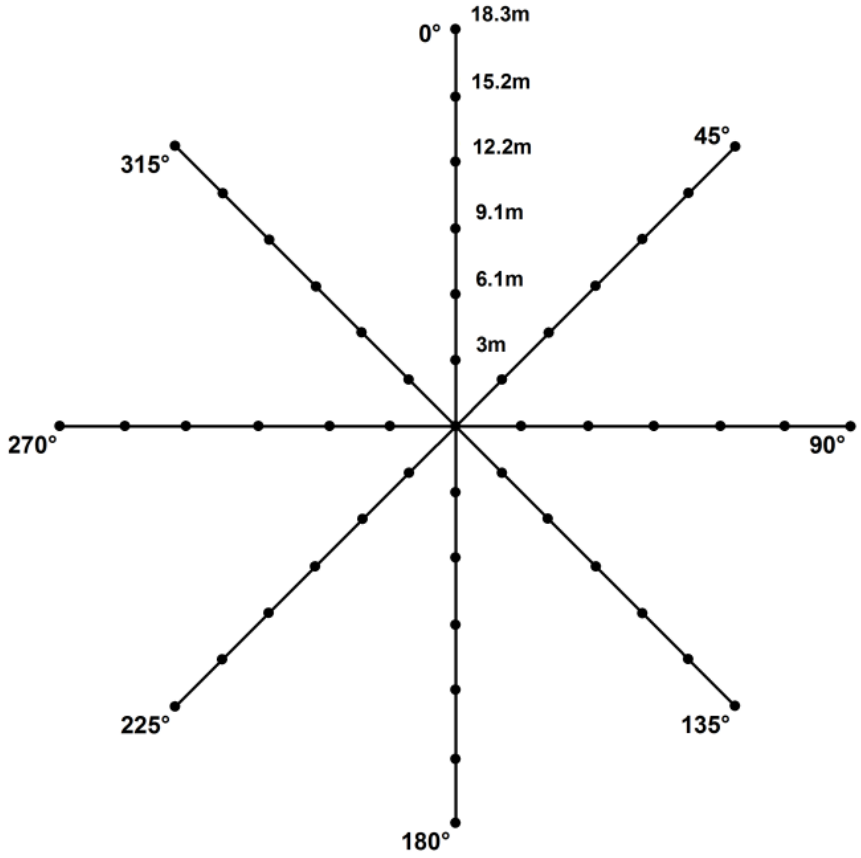

Figure 2.4. Diagram of the eight transects and six locations along transects used to collect elevation change information on each field plot.

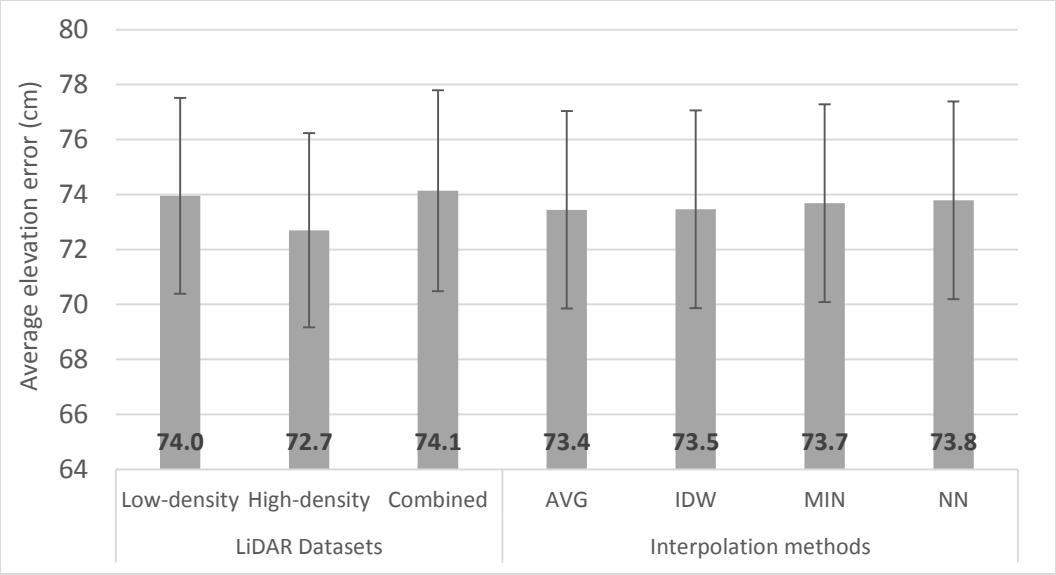

Figure 2.5. Mean elevation error averaged by LiDAR dataset and interpolation method with their respective 95% confidence intervals.

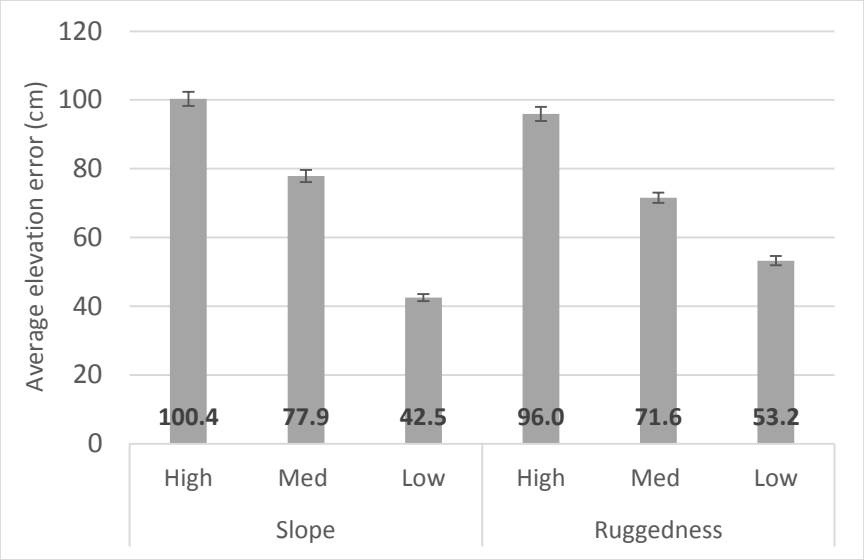

Figure 2.6. Mean elevation error by slope and ruggedness classes averaged from all LiDAR datasets and interpolation methods with 95% confidence intervals.

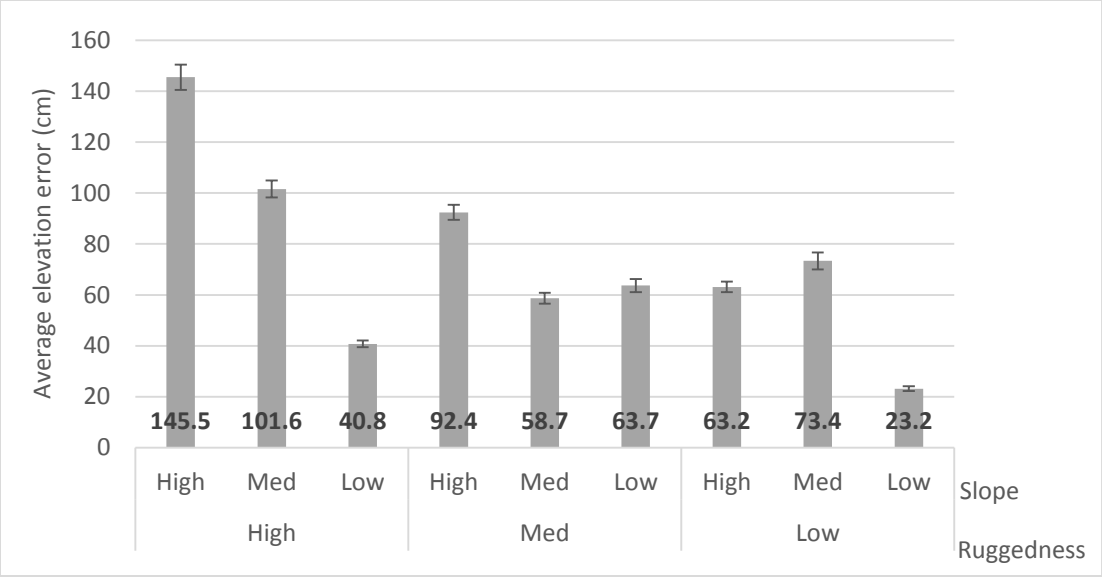

Figure 2.7. Mean elevation error by combination of slope and ruggedness classes averaged from all LiDAR datasets and interpolation methods with 95% confidence intervals.

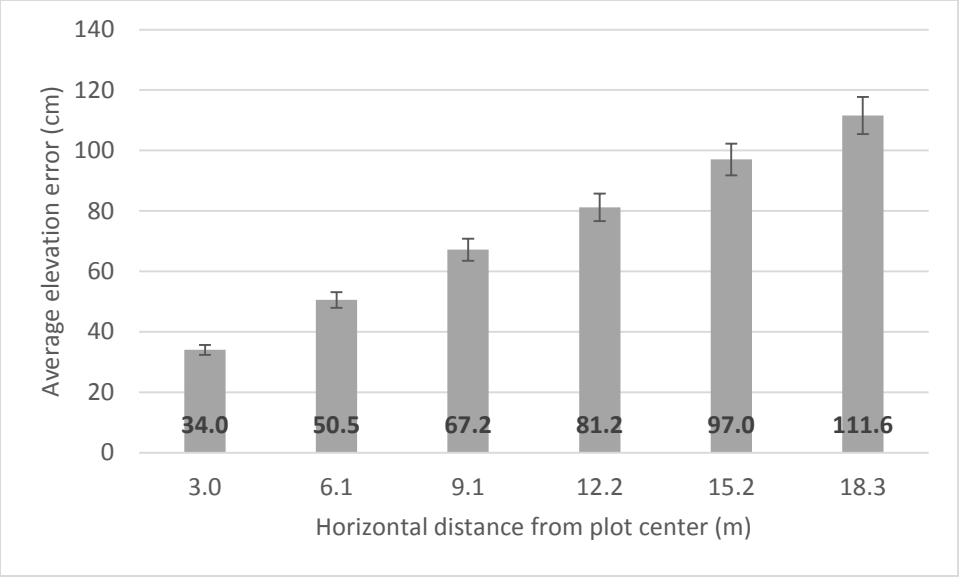

Figure 2.8. Mean elevation error by distance from plot center averaged from all LiDAR datasets and interpolation method with 95 % confidence interval.

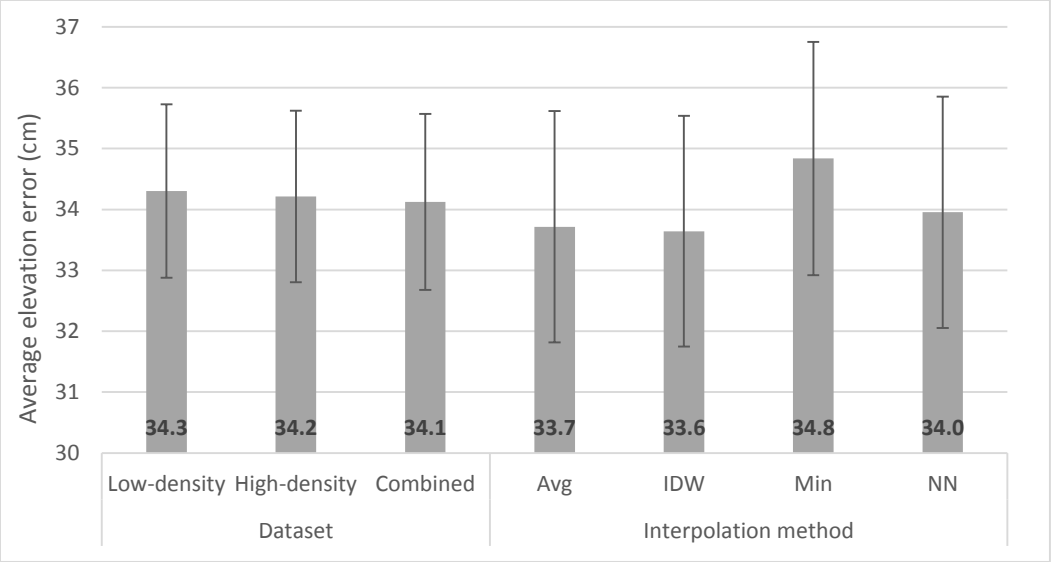

Figure 2.9. Mean elevation error averaged by LiDAR dataset and interpolation method with their respective 95% confidence intervals considering only measurements taken from points 3.0 m horizontal distance from plot center.

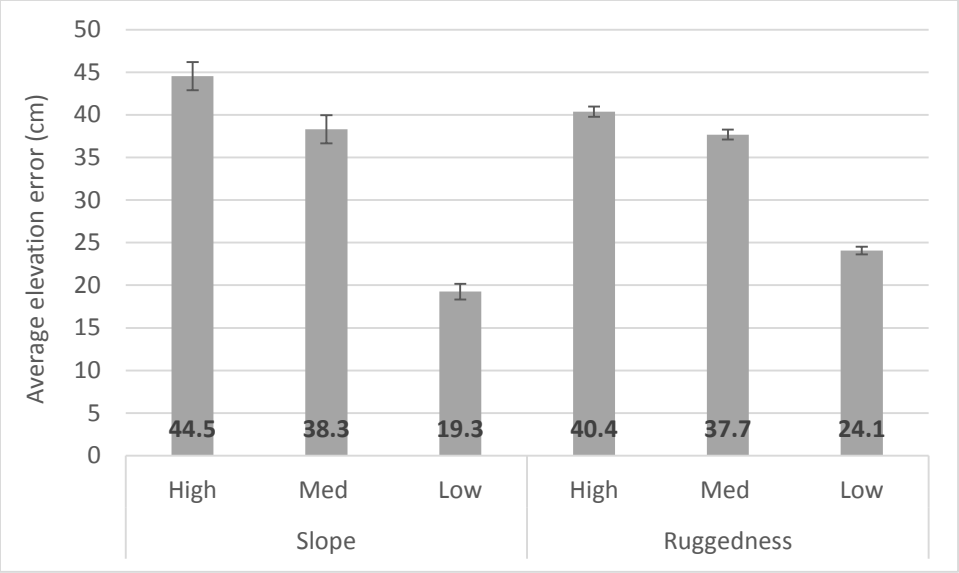

Figure 2.10. Mean elevation error by slope and ruggedness classes averaged from all LiDAR datasets and interpolation methods with 95% confidence intervals considering only measurements taken from points 3.0 m horizontal distance from plot center.

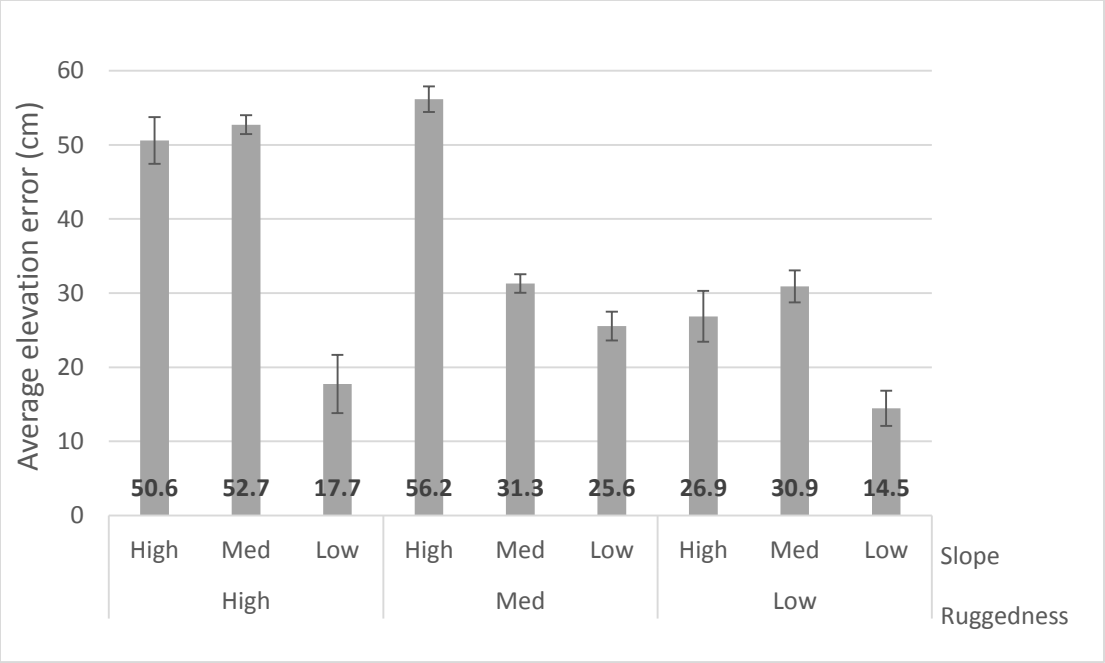

Figure 2.11. Mean elevation error by combination of slope and ruggedness classes averaged from all LiDAR datasets and interpolation methods with 95% confidence intervals considering only measurements taken from points 3.0 m horizontal distance from plot center.

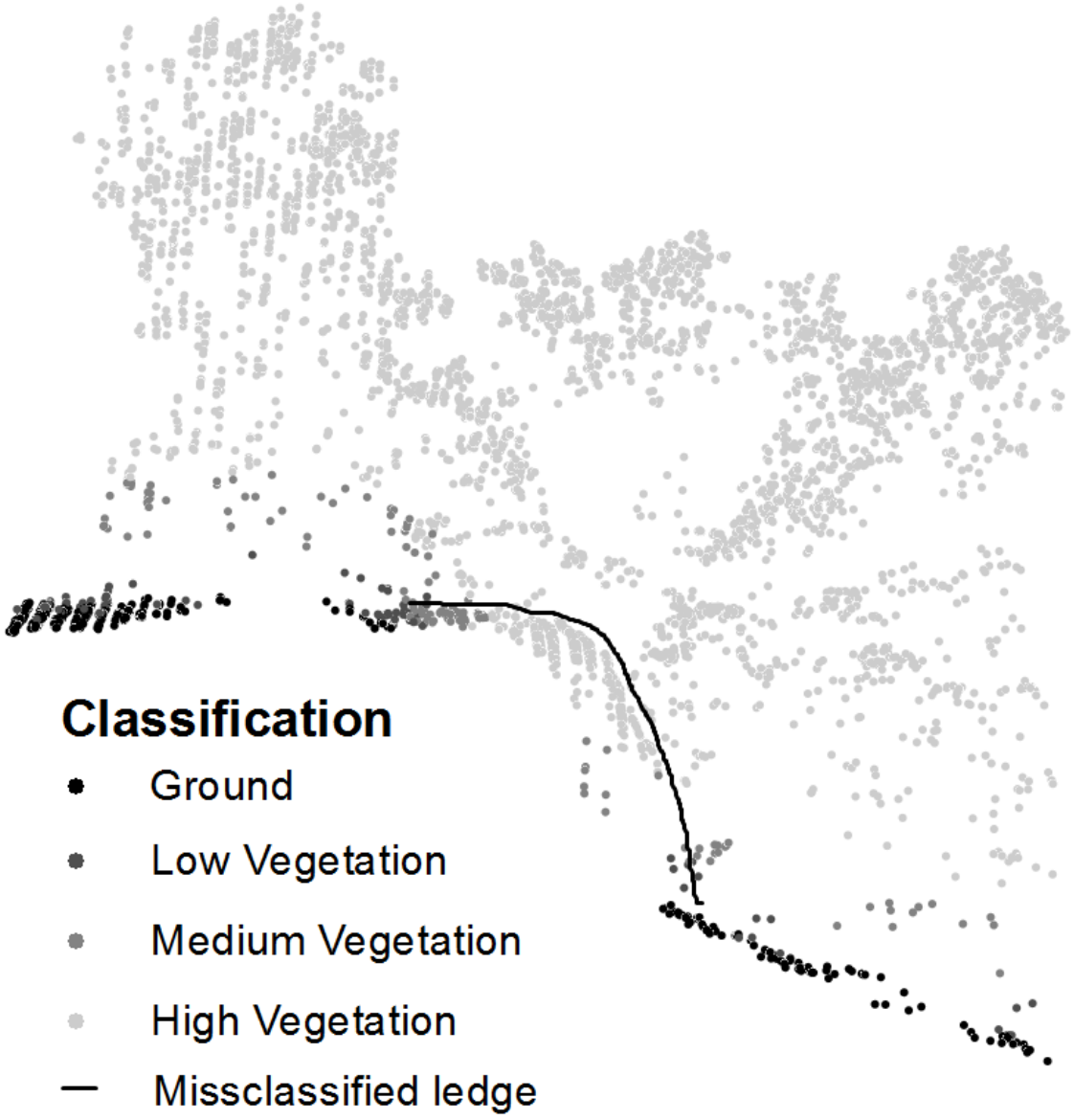

Figure 2.12. An example where LiDAR points were misclassified by the data provider. The area under the red line is classified as high vegetation and medium vegetation where it should be classified as ground points because that area is a rock ledge.

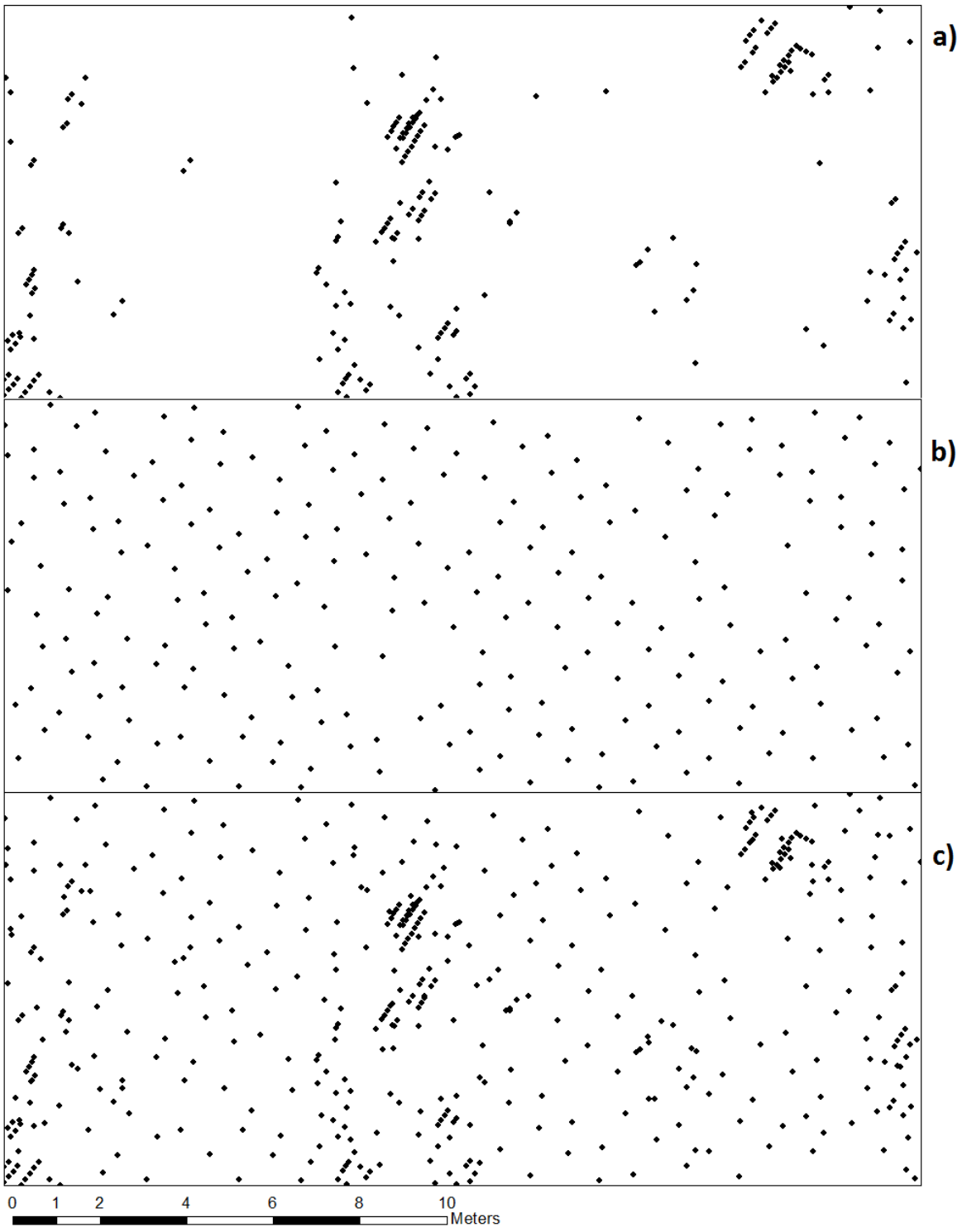

Figure 2.13. Shown is the LiDAR ground point pattern and distribution across a landscape for the high-density (a) low-density (b) and combined (c) LiDAR datasets.

	Leaf-off dataset	Leaf-on dataset
Date of acquisition	April 23, 2013	May 28- 30, 2013
LiDAR system	Leica ALS60	Leica ALS60
Average flight elevation above ground	3,096 m	1,305 m
Average flight speed	105 knots	105 knots
Scan frequency	200 kHz	200 kHz
Scan angle	< 40^{o}	< 40^{o}
Overlap between adjacent strips	50%	50%
Average swath width	701 m	183 m
Maximum number of returns captured	3	5
Average footprint diameter	0.25 m	0.1 m
Nominal pulse spacing	< 1.0 m	< 0.2 m

Table 2.1. LiDAR data acquisition parameters used for both datasets collected over Robinson Forest.

			Slope			
			Low (0 – 39 %)	Medium (40 – 50 %)	High (50 – 103%)	Total
Ruggedness	Low	(0 – 28 %)	81.7	257.4	205.4	544.5
	Medium	(28 – 45 %)	207.4	201.1	219.8	628.2
	High	(46 – 103 %)	301.7	157.7	164.5	624.0
	Total		590.8	616.2	589.7	1796.7

Table 2.2. Area (ha) under each combination of slope and ruggedness category considered to randomly select field plots to collect surface terrain information.

Ruggedness	Slope	Leaf-off, low-density (1 pt m^{-2})				Leaf-on, high-density (40 pt m^{-2})				Combined			
		AVG	IDW	MIN	NN	AVG	IDW	MIN	NN	AVG	IDW	MIN	NN
High	High	145.7	145.7	146.1	145.7	144.9	145.0	144.1	145.9	145.5	145.6	146.1	145.5
	Med	103.8	103.9	103.7	104.3	92.0	92.0	92.8	92.2	108.5	108.4	108.8	108.7
	Low	40.6	40.7	40.6	41.5	41.1	41.3	39.8	41.8	40.6	40.6	40.5	40.3
Med	High	91.2	91.2	91.9	91.9	94.1	94.2	95.3	95.1	89.5	89.9	93.0	91.8
	Med	64.1	64.2	64.9	64.6	54.4	54.4	55.2	54.6	56.5	56.6	57.6	57.1
	Low	63.9	63.8	64.3	63.8	63.0	63.1	64.4	63.5	63.0	63.1	64.9	63.6
Low	High	63.6	63.7	64.3	64.0	64.6	64.1	65.1	63.1	61.6	61.2	61.8	60.7
	Med	68.3	68.2	67.8	68.3	77.3	77.3	74.3	77.1	76.5	76.7	71.7	77.2
	Low	22.9	23.0	22.9	23.2	21.9	21.9	23.8	22.4	23.7	23.7	24.0	24.4
Averages		73.8	73.8	74.1	74.1	72.6	72.6	72.8	72.9	73.9	74.0	74.3	74.4
		74.0				72.7				74.1			

Table 2.3. Average elevation errors (cm) associated with the nine combinations of ruggedness and slope category obtained from the twelve DEMs created using the three LiDAR dataset and four interpolation methods.

	ANOVA SS	Mean Square	F Value	PR > F
Ruggedness	89.00	44.50	30.59	<0.0001
Slope	164.55	82.28	56.55	<0.0001
Ruggedness × Slope	80.90	20.22	13.9	<0.0001
Distance	202.92	40.58	27.89	<0.0001
Ruggedness × Distance	13.47	1.35	0.93	0.5103
Slope × Distance	20.14	2.01	1.38	0.1889
Ruggedness × Slope × Distance	31.13	1.56	1.07	0.3832

Table 2.4. Three-way ANOVA using slope, ruggedness, and horizontal distance from plot center.

	ANOVA SS	Mean Square	F Value	PR > F
Ruggedness	22.37	11.19	13.51	<.0001
Slope	63.33	31.67	38.26	<.0001
Ruggedness × Slope	27.83	6.96	8.41	<.0001

Table 2.5. Two way ANOVA using slope and ruggedness considering only measurements taken from points 3.0 horizontal distance from plot center.

Chapter 3: Applications of LiDAR technology on predicting Plethodontid Salamander Abundance

Introduction

Woodland salamanders in the family Plethodontidae, are important components of Appalachian forests (Hairston, 1949) with biomass capable of surpassing all birds and small mammals combined (Burton and Likens, 1975a). Their exceptional biomass make them a key part of ecosystem function, influencing food webs by predating on insects and providing food for a variety of predators including fish, reptiles, small mammals and birds (Davic & Welsh, 2004). Hairston (1987) suggested woodland salamanders in the Appalachia are the dominant predators based on their predatory status and high caloric content. Woodland salamanders also have a large influence on soil decomposition by providing huge nutrient pools (Burton and Likens 1975b) while also consuming litter fragmenting insects (Wyman, 1998).

With such a large impact on forest ecosystems woodland salamanders should be taken in to consideration when managing forested lands. Woodland salamanders are known for their cutaneous breathing, which leaves them very sensitive to desiccation (Peterman and Semlitsch, 2014), changes in temperature effecting metabolic rates (Homyack et al., 2011), and soil acidification (Wyman and Jancola, 1992). Their environmental sensitivity, small home range, and low vagility (Welsh, and Droege, 2001) means their distributions are dependent on microhabitats and are often uneven across a landscape. Studies show that woodland salamander numbers drastically decline immediately following clearcut practices and could take up to 60 years to fully recover (Petranka, 1999; Ash, 1997) while their abundance is highest in

mature forests (Petranka et, al., 1993). Woodland salamanders in the Northern Appalachian Mountains are also experiencing declines due to leaf litter loss from non-native earthworm invasions, exacerbated by the creations of forest openings (Maerz, et al., 2009).

In order to properly account for woodland salamanders when managing land one would need to know their distribution across the landscape. Habitat modeling is often used to estimate organisms' distribution across landscapes although developing accurate landscape level habitat models for sensitive species can be difficult. Many of the models researchers develop are on a small scale and require fine scale inputs that are unavailable to land managers (Stauffer, 2002) while many landscape level models are based on generic remotely sensed variables such as vegetation type, climate, and topographic variables which are less useful for distinguishing fine scale habitat (Fleishman et al. 2001). Light Detection and Ranging (LiDAR) has advanced rapidly in the past decades and can provide much more specific fine scale information. The data provided through LiDAR are discrete point coordinate measurements of all surfaces in a landscape, achieved by flying an aircraft with a highly accurate GPS and laser range finder system over a landscape. The new technology provides high accuracy and high resolution data for both topographic and vegetation surfaces (Reutebuch et al., 2005) which allows for interpolating very fine scale topographic and vegetation metrics.

While LiDAR has been used in many natural resource applications to obtain biomass measurements (Popescu, 2007; Srinivasan et al., 2014), individual tree positions (Rahman and Gorte, 2008), tree heights, quadratic mean diameter, basal area (Goerndt et al., 2011) and other crown dimensions (Kim, 2008), there are many limitations to its use. The majority of work with LiDAR has been limited to homogenous stands of coniferous trees on terrain that is not

drastically sloped. Individual tree metrics are mostly based on delineating tree crowns which is much simpler for conifers' uniform conically shaped crowns with obvious apexes opposed to deciduous trees' irregularly rounded crowns with less obvious apexes. Deciduous forests such as the southern Appalachian Mountains contain many different species with varying crown shapes making it even harder to obtain accurate forest metrics for individual trees, which is why researchers haven't been able to develop as useful LiDAR techniques for vegetation based habitat variables in this area.

This study uses a method of using area based techniques for interpolating LiDAR data in a complex deciduous forest of the Southern Appalachian Mountains to describe fine scale vegetation and topography metrics such as canopy cover vegetation height and vegetation height standard deviation, slope's exposure to light, and water flow accumulation; all of which might affect the local abundance of salamanders. We focused on two similar species of woodland salamander, the Slimy Salamander (*Plethodon glutinosus*) and the Cumberland Plateau salamander (*Plethodon kentucki*). We hypothesize that individuals will be more abundant in moist lower slopes with fully closed canopies and less direct topographic exposure to the sun based on their sensitivity to desiccation (Peterman and Semlitsch, 2014) and previous finding by Peterman and Semlitsch, (2013). The study methods are meant to be replicable for other deciduous forests in the United States and for other amphibian species. The results could be used to identify ideal habitat for different species, and to locate areas to focus management practices.

Methods

Study area

Research was conducted at The University of Kentucky's Robinson Forest, located in the Cumberland Plateau region of southeastern Kentucky (Lat. 37.4611, Long. -83.1555). Due to access restriction and to reduce travel time between field plots, the study area was limited to the 1550 ha Clemons Fork watershed (Figure 3.1). The study area and the entire Robinson Forest is comprised of a diverse contiguous mixed mesophytic forest made up of over 80 tree species (Carpenter et al., 1976) with oak and maple being the dominant overstory trees. After being extensively logged in the 1920's, Robinson Forest is considered second growth forest ranging from 80-100 years old, and is now protected from commercial logging and mining activities, typical of the area (Overstreet, 1984). The topography is steep with short benched and dissected slopes, elevation ranges from 250 to 503 meters above sea level, slopes range from 0 to 100 percent, and aspects facing all directions (Overstreet, 1984). Average canopy cover across Robinson Forest is about 93% with small opening scattered throughout. Most areas exceed 97% canopy cover but recently harvested areas have an average cover as low as 63%. The forest is home to 17 species of salamander, most of which belong to the family Plethodontidae. (Schneider, 2011; Petranka, 1998). The most abundant terrestrial salamanders from our field sampling are *Plethodon glutinosus* and *Plethodon kentucki*, which are the focus of this study. Both of these salamanders' are lungless salamanders (they breathe cutaneously) and thus prefer cool moist habitats and are most active on the surface of the ground, at night, after rain events (Petranka, 1998)

Sampling design

To quantify the abundance of salamanders, 45 field transects were surveyed across varying soil moisture and canopy cover conditions throughout the study area (Figure 3.2). A geographic information systems (GIS) based integrated soil moisture index (Iverson et al., 1997) was developed to determine soil moisture, which takes into account hillslope, direct sun exposure (hillshade), ground curvature, and soil water holding capacity data from the United States Geological Survey (USGS). The GIS layer was a 10 m cell size raster expressing relative soil moisture across Robinson Forest. The raster was resampled into coarser 30.5 m (100 ft) cells using the average of the smaller cells to match the size of transects and encompass them into single cells. The raster was classified in to high, medium, and low soil moisture classes selecting threshold values resulting in an equal amount of area in each class (516.7 ha). Canopy cover was determined using a high-density (~ 40 pt m^{-2}) LiDAR dataset acquired in the summer of 2013 during leaf-on season for the purpose of collecting detailed vegetation information. The parameters of the LiDAR system and flight are presented in Table 3.1. The raw 3D LiDAR point cloud was used to calculate canopy cover as the percentage of vegetation points above 5 m from ground level to the total points for each 0.6 m (2ft) cells throughout the Robinson Forest. If this percentage was greater than 50 %, then the cell was considered covered and given a value of 1, if the percentage was below 50%, the cell was considered not covered given a value of zero. This 0.6 m (2ft) raster layer was then aggregated into 30.5 m (100 ft) by averaging to cover the intended field plot sampling area. The canopy cover raster was then classified in to three classes where 0 to 50 percent covered was considered low, 50 to 75 medium, and 75 to 100 high canopy cover. Lastly, five transects were randomly placed in each

combination of soil moisture and canopy cover using the center point of the raster cells as the transect locations. Transect locations avoided areas 5m from existing roads, skid trails and streams to limit their effects on observed salamanders.

In field Data collection

The location of transects was established using a Trimble Juno SB GPS handheld unit with a precision of 6 m (20ft) from given coordinates (center of raster cells). Plot locations were used as the mid-point of 30.5m (100ft) transects layout along the contour line. Flagged were installed at the ends and mid-point of transects to establish a clear line of sight along the transect length. Transects were surveyed at night time using a visual encounter survey (Flint and Harris,2005; Grover, 2006) on days following rain events during May – June of 2014. Transects were surveyed using a neutral white Zebralight H600w Mk II headlamp searching the transects over a 1m (3.3 ft) swath along either side of its length. Encountered salamanders were captured, placed in Ziploc bags, and left at the same place they were found along the transects to minimize disturbance to the site. After the full transect was searched, limiting search time to 30 minutes, captured salamanders were then examined and species was recorded.

All sites were sampled three times, as multiple visits are required for presence and abundance modeling (Royle 2004; Mackenzie et al., 2002) to account for detection probabilities. Transect locations were grouped where several could be accessed in one night, then groups were randomly surveyed with no transects being revisited within three days of the last survey. Site specific variable that could affect desiccation rates and salamander detection (Peterman and Semlitsch, 2014). were also recorded such as wind speed, barometric pressure

(mmHg), air temperature (°C) using a Kestrel 2500 weather meter, soil moisture (%) using an Extech MO750 soil moisture probe, litter depth (cm), and Julian date. Other detection variables obtained from a permanent weather station at the study site include days since last rain event, last rain amount (cm), and average humidity (%).

Lidar derived data

For the purpose of predicting and mapping salamander abundance across Robinson Forest, a set of LiDAR-derived predictive variables were obtained. First, a DEM was created using the LAS dataset tool in ArcMap 10.2 and filtering the LiDAR points to include only points representing the ground. Within ArcMap, the "LAS dataset to Raster" tool was used to create a 0.6 m resolution DEM using average as the cell assignment method and natural neighbor as the void fill method. Predictive variables based on the LiDAR-derived DEM included five raster layers representing: hillshade, flow accumulation (FA), vegetation height (VH), vegetation height standard deviation (VHSD), and the previously mentioned canopy cover (CC) layer. As aforementioned, the hillshade layer is a proxy for the amount of direct sun exposure and was created using the known sun position (175° azimuth and 70° altitude) for the time field data was collected. The flow accumulation represents the number of upslope cells theoretically flowing onto a given cell and is an indication of relative humidity. Vegetation height was calculated by subtracting the DEM from the digital surface model (DSM) to represent elevation above ground level. The DSM represents elevation of the top of the canopy above sea level and it was created similarly to the DEM using the LASTools extension but by filtering LiDAR points to include only first return points. The vegetation height standard deviation layer was calculated as the standard deviation of the vegetation height of 0.6m (2ft) cells within coarser 30.5 m (100

ft) cells. It was created to represent the variability of heights which would tend to be higher in areas that recently underwent timber harvesting and would be lower in areas with fully closed canopies. As aforementioned, all raster layers were resampled to a coarser resolution of 30.5 m (100 ft) to unify their resolution and to consider a cell size more appropriate to meaningfully capture site variations across the study site.

Data analysis

To maintain consistency with the resolution of raster layers representing the predictive variables, a 15.2m (50 ft) buffer was placed around each transect covering 0.17ha. This buffer area was then used to extract a single value for each of the predictive variables representing each transect. Predictive models were then developed to estimate salamander abundance based on the set of predictive variables previously mentioned. Due to the large amount of transect surveys yielding no salamander observations, we used the statistical function RunZIA (Wenger, 2007; Wenger, and Freeman, 2008) in R version 3.1.1 (R Development Core Team, 2008) to run zero inflated models to obtain multiple linear regression model parameter estimates. The RunZIA function was designed based on Royle's n-mixture model (Royle 2004, Royle et al. 2005) which predicts abundance based on multiple visits to sites. RunZIA also incorporates a model by Mackenzie et al. (2002) which uses detection variables to account for differences in detection probability during each site visit to determine occupancy. RunZIA's combination of these two approaches calculates abundance given that a site is first occupied, and estimates abundance at the site based on a Poisson distribution. The RunZIA function also uses detection probabilities based on sampling covariates when predicting whetehr the site is occupied. The full predictive model can be explained by the equation below where N_i is the

realized abundance at site i given presence, $pres_i$ is a binary value expressing whether salamanders are present at site I, ψ is the probability that the species is present at the site and k_i is the predicted abundance at site i.

$$N_i = pres(\psi_i) \times k_i$$

The model outputs can be used to predict salamander abundance across the landscape, assuming constant detection probability by using the equations below to transform the model output parameter estimates and applying them to the equation above.

$$pres_{i =} BIN(\ EXPIT(\beta_o + \beta_1 X_{1\ \ldots +}\ \beta_i Xi))$$

$$k_i = EXP\ (\beta_o + \beta_1 X_{1\ \ldots +}\ \beta_i Xi)$$

All models for this study were run using the original variable units instead of using a Z-score standardization in order to apply the parameter estimates to values for the entire Robinson Forest to make a predictive map of abundance. Additionally, all models included both the Julian date and the squared days since last precipitation date as sampling covariates for detection probability because seasonal and weather variables greatly influence desiccation rates of salamanders and have been shown to affect their surface activity and detection probability (Petranka, 1998; Peterman and Semlitsch, 2014). These two variables have been shown to explain most of the variability within our recorded observations compared with the other sampling covariates measured in the field. The same variables were run as both abundance predictors and presence (occupancy) predictors for each model and included either a topographic variable (soil moisture index, flow accumulation, hillshade) or vegetation variable (canopy cover, vegetation height, vegetation height standard deviation) or combination of

both. Values for FA were restricted from 0 to 149 m2 where 0 value cells occur on ridgetops and 149 m2 occur close to a stream while values greater than 149 m2 indicate a presence of a stream. Values of VHSD range of 0 to 9 m where 0 could be an area with no vegetation and 9 would be an area with highly variable tree heights. The same models were run separately for both *Plethedon glutinosus* and *Plethedon kentucki* to determine if there were differences in site preference between species. Models were ranked based on the small sample size Akaike information criterion (AICc) and the evidence ratio (ER), and the weighted Akiake criterion (W AICc) was used to determine the relative performance of the best model (Symonds and Moussalli, 2011).

Results

Plethodon glutinosus and *Plethodon kentucki* were the most observed species, with a total of 63 and 99 observations respectively out of a total of 184 salamander observations from 3 visits to each transect. There were no salamanders observed in 85 visits out of the total 135 visits, which justified the use of a zero-inflated model to describe salamander abundance. Before models were tested, a Pearson's correlation matrix was run to examine the relationship among LiDAR-derived predictive variables (Table 3.1). Results indicate a relatively high correlation between canopy cover and vegetation height (r = 0.89) as well as between soil moisture index and hillshade (r =-0.81), so those variable were not combined within any of the models.

We ran several models with different combinations of LiDAR-derived covariates to predict *Plethodon glutinosus* abundance (Table 3.2). Results show that the best fit model contained VHSD and FA. Based on the evidence ratios, the selected model has evidence to

perform better over 26 times stronger than the next highest ranked model. This model is also over 95% more likely to perform better than the next highest ranked model based on the weighted Akiake criterion. VHSD and FA are also present in most of the other highest ranked models and are therefore very likely to influence Plethodon glutinosus abundance. When examining the parameter estimates and their 95% confidence intervals for the complete best fit model (Table 3.3), none of the intervals of the abundance parameter estimate overlap zero, which indicates that the respective variables are likely to be important in the model. The negative estimate for VHSD indicates an inverse affect on abundance while FA has a direct affect, but for the presence portion of the model the both covariates have a direct effect. Figure 3.3 shows the best fit model for *Plethodon gultinosus* applied to real world values for Robinson Forest. The values ranges from 0 to 1.64 individuals per m^2 with a mean value of 0.12. This model predicts a high concentration of individuals located close to ephemeral streams in the head waters while sparsely distributed elsewhere, and shows that the FA variable has a greater visible effect than VHSD.

Models run with different combinations of LiDAR-derived variables to predict the abundance of *Plethodon kentucki* (Table 3.4) show a less clear best fit model, however six of the top seven models contain canopy cover and the top model with only canopy cover as the abundance presence variable is 48 percent more likely than the rest to be the most accurate. In the best fit model the canopy cover's parameter estimate (Table 3.5.) for abundance was positive, indicating a direct relationship to abundance. The 95% confidence interval does not overlap zero, which additionally indicates that it is an important variable for this species. Canopy cover's parameter estimate for abundance was also positive but has a confidence

interval greatly overlapping zero which indicates that this variable may not be important for predicting presence. When the model is applied to CC information for Robinson forest (Figure 3.4) abundances range from 0.04 to 0.82 individuals per m^2 with an average of 0.58 individuals per m^2. This model did not predict that any areas were unoccupied for *Plethodon kentucki*, only a reduced abundance with low CC while their abundance is more evenly spread across the forest. This is likely why the average is so much higher than *Plethodon glutinosus* (0.58 vs 0.12 individuals per m^2).

When comparing these two species, results show that different LiDAR-derived covariates have a significant effect on their abundance. For example, VHSD is retained in almost all high ranked models (AICc < 218) for *Plethodon glutinous* abundance, while CC is retained in most low ranked models (AICc > 218) (Tables 2 and 4). The opposite case can be observed for *Plethodon kentucki* where CC and VHSD are retained in high (AICc < 279.1) and low-ranked (AICc > 279.1) models respectively. When applying the best abundance / presence model to the map abundance across the study area, it can be observed that *Plethodon glutinosus* is predicted to be present in high numbers closer to streams while not occupying ridgetops, which makes it clear that flow accumulation is affecting abundance most in this model (Figure 3.3). However, *Plethodon kentucki* is predicted to have high abundances throughout except for roads surfaces and recently harvested areas with low canopy cover (Figure 3.4). The abundance map for the Plethodon kentucki is extremely similar to the map of canopy cover for the study site because canopy cover is the only variable represented in that model.

Discussion

This study is a good starting point for quantifying salamander abundance using fine scale vegetation and topography information derived from LiDAR in a deciduous forest. These methods could be replicated by land and wildlife managers for different species of terrestrial Plethodontid salamanders or slightly modified for other amphibians to determine what factors most effect their distribution across the landscape and to model their relative abundance. Our two models reasonably predict salamander abundance when compared to the field observations and the output of two different best fit abundance models for the two similar Plethodontid species is further evidence that the vegetation and soil characteristics extracted from the LiDAR data are of high enough accuracy and resolution to describe minute differences in habitat preference between the two species. In figure 3.3 and 3.4 we can see that the two species are distributed differently across the landscape and have different ranges of abundance. Our models are also likely representative because they output similar abundances to studies such Marvin's (1996) study which found <0.2 *Plethodon kentucki* per m^2 compared to our average predicted 0.58 *Plethodon kentucki* per m^2. Semlitch (1980) found 0.52- 0.81 *Plethodon glutinosus* compared to our average predicted .12 *Plethodon glutinosus*.

While the best fit models were fairly accurate, they are oversimplified and include only one or two main variables to predict abundance and presence. Peterman and Semlitsch, (2013) conducted a similar study for another terrestrial salamander, *Plethodon albagula* and found importance for factors such as canopy cover, ravine habitat, solar exposure, and topographic wetness in there best model. It is likely that many of these factors also have an effect on our species. In addition, our models were solely based on the known phenomena of desiccation

effecting salamander activity and abundance (Peterman and Semlitsch, 2014), however it is also well understood that salamanders' abundance and presence are also affected by forest age (Petranka, 1998; Petranka, 1999), which would likely be beneficial in this modeling. While it is difficult to quantify forest age over large landscapes, basal area or the diameter at breast height (DBH) of trees could be used as surrogate predictive variables for age and have been calculated over large landscapes using LiDAR data in coniferous forests. These were not included in our study because this information is much harder to estimate in deciduous forests due to the trees' irregularly rounded crowns (Popescu, 2007).

Our best model for *Plethodon kentucki* predicted an almost constant high abundance throughout the forest (figure 3.4), which we believe is not a true representation of the species. Even though many more of our field sites had observations for *Plethodon kentucki* vs *Plethodon glutinosus* there were still many zero count plots for *Plethodon kentucki*. While canopy cover has shown to have a strong effects on terrestrial salamander abundance (Peterman and Semlitsch, 2014) we believe there are further topographic components effecting these salamanders' abundance (Peterman and Semlitsch, 2013, Peterman and Semlitsch, 2014). Thus, it is likely that either we have not fully represented the variables effecting salamander distribution in our study site.

Unaccounted for biotic factors could also be influencing our species abundances. Species interactions are important in species distributions across environmental gradients (Gifford and Kozak, 2012) and could likely make narrowing down optimal ranges of environmental conditions for sympatric species difficult. While both of these species were present together at many of the same plots *Plethodon glutinosus* has been known to

aggressively defend its territory (Thurow, 1976) and competitive interactions are likely to occur between the two species (Marvin, 1998). Other territorial species such as the green salamander (*Aneides aeneus*) (Cupp, 1980) are also present in the area and could be further confounding the effort to quantify the abiotic environmental effects. The lack of other terrestrial Plethodontid salamanders in Peterman and Semlitsch's (2013) study could have allowed them to develop more complex models.

Some of the inaccuracy of this study could be due to how the field sites were selected and how the data was collected. The study was based on quantifying desiccating effects and therefore we needed to represent areas with lower canopy cover, but because the study site is almost entirely second growth continuous forest there weren't many areas with low canopy cover. Recently harvested areas were the only option to sample when representing medium and low canopy cover and therefore most of the field plots occurred in recent timber harvests. Both species' best fit models contained some form of a vegetation variable, which predicted lower abundance in those areas, however while that could be due increased desiccation from more direct sunlight via canopy openings, it could also be due to recent disturbances from logging lowering the populations or other indirect effects from logging. In retrospect randomly placing field plots across the landscape, ignoring canopy cover, may have produced better models because the field observations wouldn't have contained as many zero count plots. The field data collection could have also been improved by adding more plots and further limiting the data collection days to occur closer to rain events to ensure more salamander surface activity.

Conclusion

This study describes a useful method for predicting salamander abundance across a landscape that requires minimal field work paired with fine scale landscape wide habitat information to predict relative salamander abundance in a way useful for managers. This study also demonstrates the usefulness of high density LiDAR data in an area where LiDAR's use is currently limited. While these method aren't refined enough to estimate population size, they are adequate to describe relative abundance across a landscape. This could be very useful for land managers to identify important abundance predictor variables for different species, to identify areas highly abundant in salamanders to avoid disturbing, or to identifying areas for restoration. While our best models may not describe all variables affecting salamander abundance they do elucidate some of the patterns of variability our study species experience. These methods could be improved by assessing other variables besides those that might affect desiccation rates however it would require more development of LiDAR data derivation techniques to estimate other fine scale habitat information such as basal area and DBH. Future work could also focus on better ways of accounting for biotic interactions across the landscape.

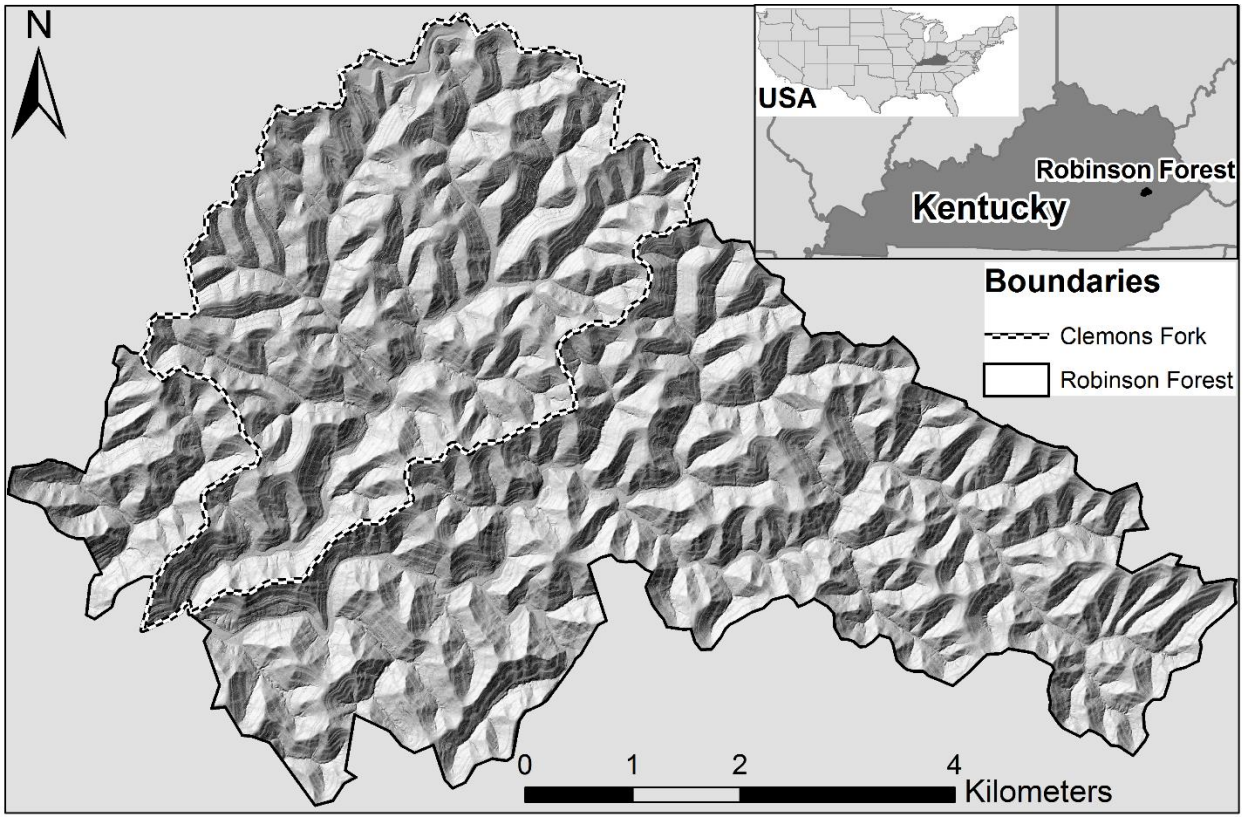

Figure 3.1. Topography of the study area (1,400 ha) within Robinson Forest (4,250 ha) located in Breathitt, Knott, and Perry counties in southeastern Kentucky (Lat. 37.4611, Long. -83.1555).

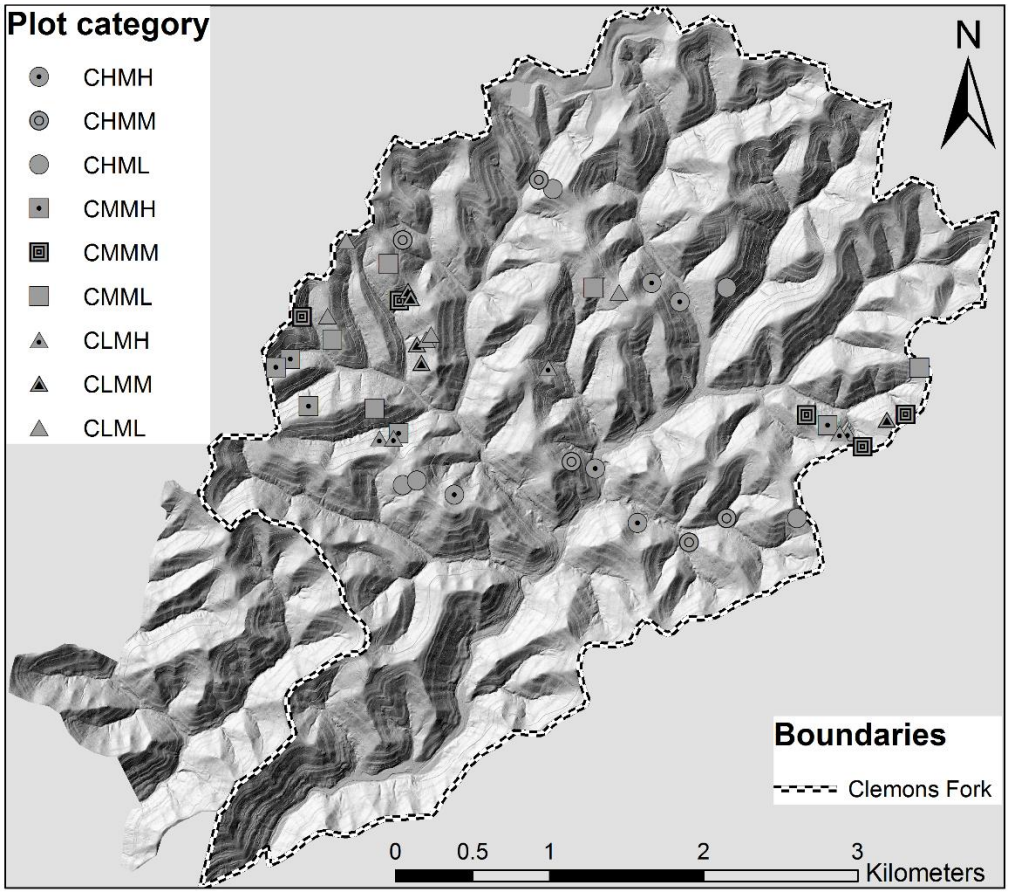

Figure 3.2. Location of field plots within the study area. First two letters in the abbreviated plot categories indicates level of canopy cover and the second two letters indicates level of soil moisture.

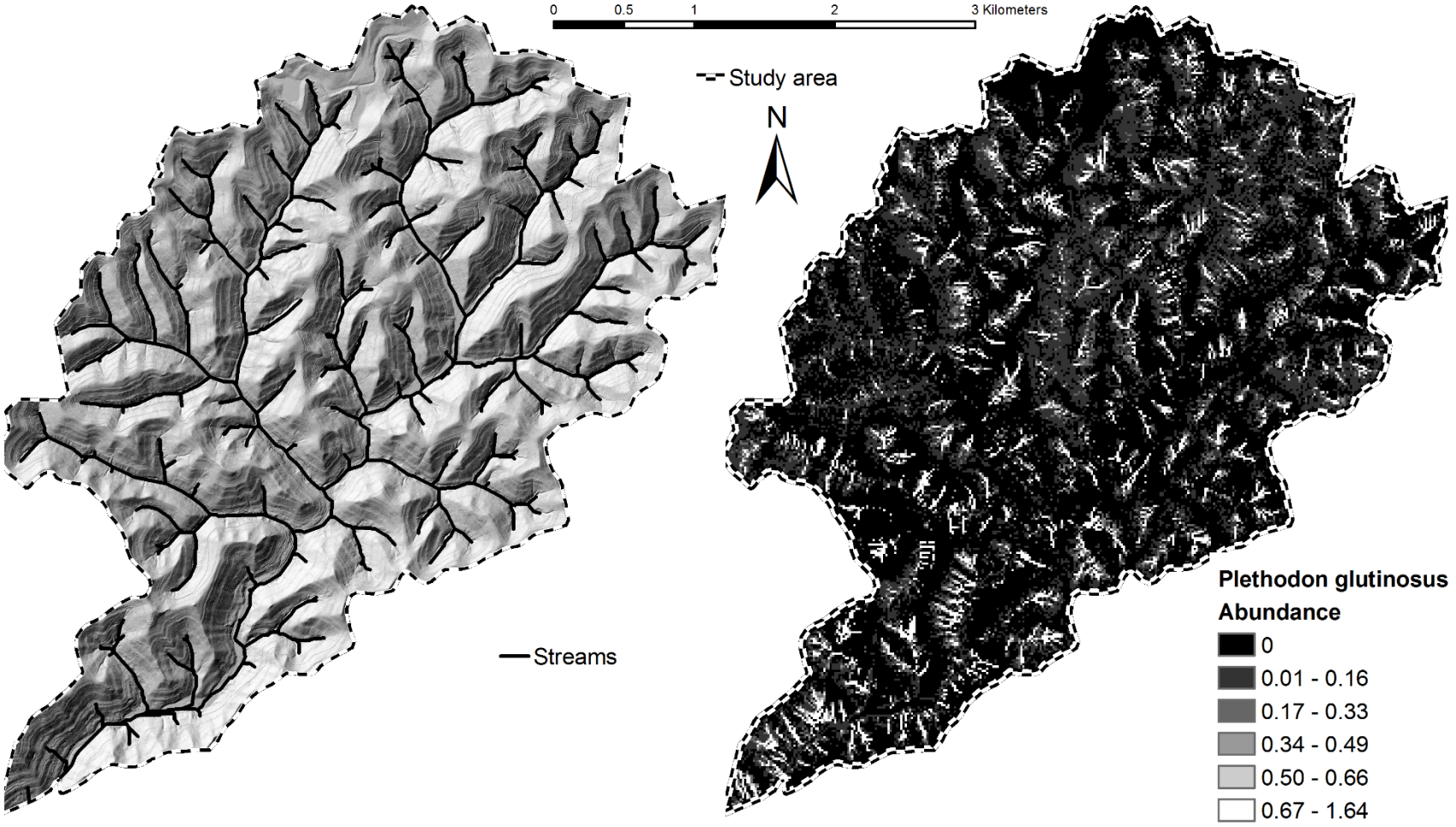

Figure 3.3. Predicted abundance of *Plethodon glutinosus* (right) expressed as individuals per m^2 and topography (left) for Robinson Forest.

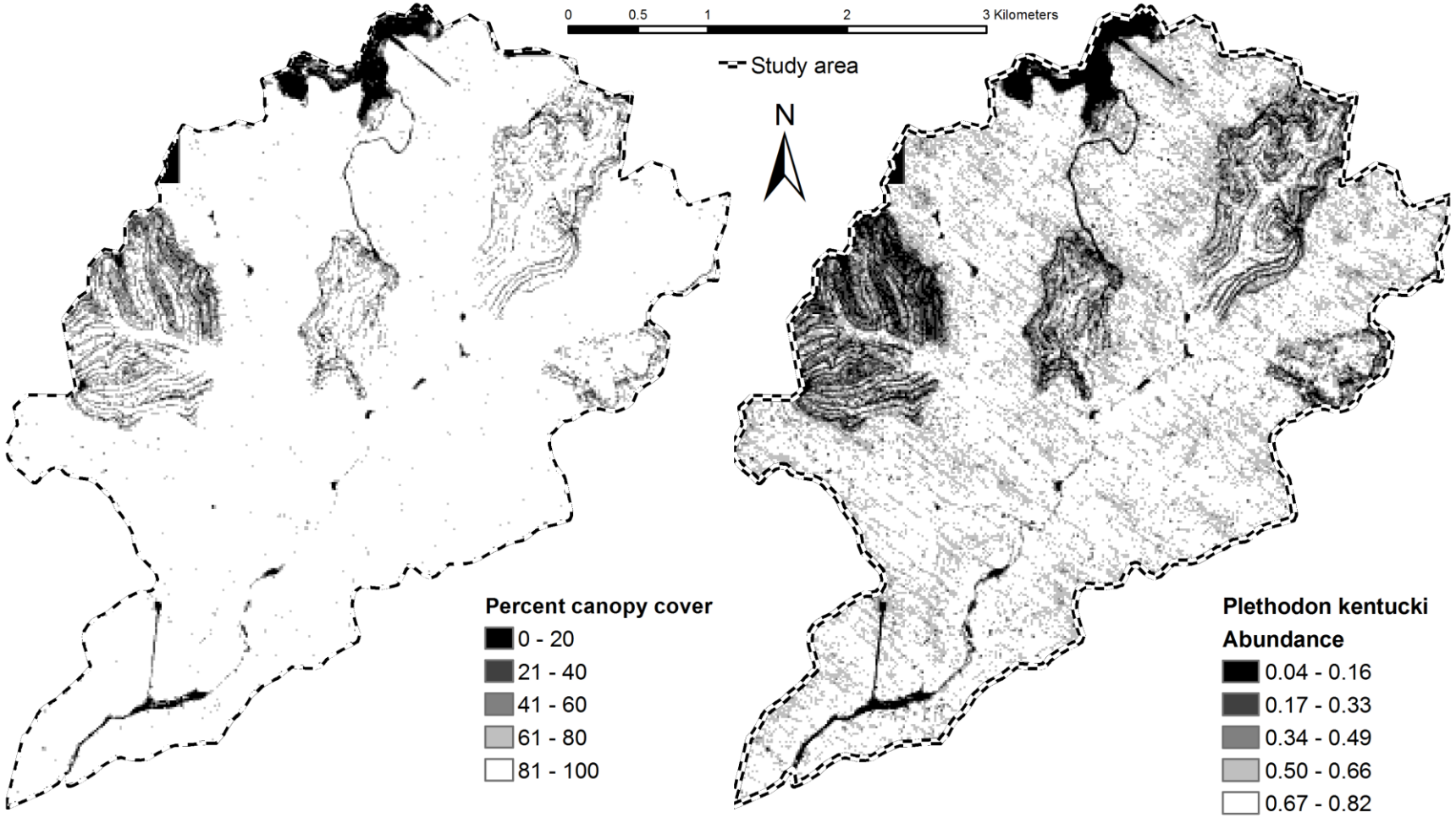

Figure 3.4. Predicted abundance of *Plethodon kentucki* (right) expressed as individuals per m^2 and percent canopy cover (left) for Robinson Forest.

	Canopy cover	Vegetation height	Vegetation height STD	Flow accumulation	Hill shade	Soil moisture index
Canopy cover	1	0.892436	0.099068	-0.01243	-0.0612	0.067231
Vegetation height	0.892436	1	0.253177	0.084228	-0.04654	0.106393
Vegetation height STD	0.099068	0.253177	1	0.105634	-0.27378	0.264318
Flow accumulation	-0.01243	0.084228	0.105634	1	-0.21542	0.415764
Hill shade	-0.0612	-0.04654	-0.27378	-0.21542	1	-0.81169
Soil moisture index	0.067231	0.106393	0.264318	0.415764	-0.81169	1

Table 3.1. Pearson's correlation matrix for variables used in model building for both salamander species.

Abundance/ presence variables	AICc	ER	W AICc
Vegetation height standard deviation , Flow accumulation	199.7776	1	0.957597
Vegetation height standard deviation , Hillshade , Flow accumulation	206.3103	26.2155	0.036528
Flow accumulation	211.2727	313.422	0.003055
Vegetation height standard deviation , Hillshade , Flow accumulation	214.1272	1306.1	0.000733
Vegetation height standard deviation	214.3194	1437.84	0.000666
Canopy cover , Vegetation height , Hillshade	215.6666	2820.02	0.00034
Canopy cover , Vegetation height , Flow accumulation	215.7841	2990.66	0.00032
Vegetation height standard deviation , Vegetation height	216.133	3560.66	0.000269
Vegetation height	216.2227	3723.99	0.000257
Soil moisture index	218.2624	10325.8	9.27E-05
Canopy cover , Hillshade , Flow accumulation	219.5593	19748.8	4.85E-05
Hillshade , Flow accumulation	220.6609	34257.1	2.8E-05
Canopy cover , Vegetation height	220.901	38626.7	2.48E-05
Hillshade	221.194	44721.1	2.14E-05
Canopy cover	221.9623	65666.9	1.46E-05
Canopy cover , Flow accumulation	225.1503	323305	2.96E-06
Canopy cover , Hillshade	226.1265	526733	1.82E-06

Table 3.2. Model ranking for Plethodon glutinonsus, showing variables used, Akaike's information criterion (AICc), evidence ratio (ER), and weighted AICc (W AICc)

Variable/ intercept	estimates	-95% CI	+95% CI
Abundance intercept	4.186	2.675	5.697
Vegetation height standard deviation	-0.117	-0.171	-0.063
Flow accumulation	0.006	0.003	0.009
Presence intercept	-19.72	-37.619	-1.821
Vegetation height standard deviation	0.831	0.022	1.640
Flow accumulation	0.026	-0.003	0.055
Detection intercept	10.392	3.31	17.474
Julian date	-0.09	-0.141	-0.039
Days since last precipitation squared	-0.138	-0.247	-0.029

Table 3.3. Parameter estimates standard error and 95% confidence interval for the best model for *Plethodon glutinosus*.

Abundance/ presence variables	AICc	ER	W AICc
Canopy cover	269.8783	1	0.476514
Canopy cover , Vegetation height	270.5098	1.37129	0.347494
Canopy cover , Vegetation height , Hillshade	272.885	4.49673	0.105969
Canopy cover , Hillshade	275.5739	17.2498	0.027624
Vegetation height standard deviation	276.5952	28.7446	0.016578
Canopy cover , Vegetation height , Flow accumulation	278.0678	60.0243	0.007939
Canopy cover , Hillshade , Flow accumulation	279.1098	101.064	0.004715
Vegetation height standard deviation , Flow accumulation	279.2361	107.652	0.004426
Vegetation height	279.272	109.601	0.004348
Vegetation height standard deviation , Vegetation height	280.8964	246.916	0.00193
Soil moisture index	282.0065	430.135	0.001108
Vegetation height standard deviation , Hillshade , Flow accumulation	282.0213	433.33	0.0011
Vegetation height standard deviation , Hillshade , Flow accumulation	285.7946	2858.78	0.000167
Flow accumulation	287.6515	7234.38	6.59E-05
Hillshade	289.9006	22273.4	2.14E-05
Hillshade , Flow accumulation	294.2767	198630	2.4E-06

Table 3.4. Model ranking for *Plethodon kentucki*, showing variables used, Akaike's information criterion (AICc), evidence ratio (ER), and weighted AICc (W AICc).

Variable/ intercept	estimates	- 95% CI	+ 95% CI
Abundance intercept	0.873	-0.775	2.522
Canopy cover	2.886	1.280	4.493
Presence intercept	0.341	-3.414	4.096
Canopy cover	0.530	-3.932	4.992
Detection intercept	3.527	-2.025	9.079
Julian date	-0.044	-0.084	-0.005
Days since last precipitation squared	-0.691	-1.003	-0.379

Table 3.5. Parameter estimates standard error and 95% confidence interval for the best model for *Plethodon kentucki*.

References

Aguilar, F. J., and Mills, J., 2008. Accuracy assessment of LiDAR-derived digital elevation models. *The Photogrammetric Record*, 23 (122), 148-169.

Alho, P., Hyyppä, H., and Hyyppä, J., 2009. Consequence of DTM precision for flood hazard mapping: A case study in SW Finland. *Nordic journal of surveying and real estate research*, 6 (1), 21-39.

Anderson, E.S., Thompson, J.A. and Austin, R.E. 2005. LiDAR density and linear interpolator effects on elevation estimates. *International Journal of Remote Sensing* 26, 3889–900.

Arun P.V., 2013. A comparative analysis of different DEM interpolation methods. *The Egyptian Journal of Remote Sensing and Space Science* 16(2):133-139.

Ash, A. N. 1997. Disappearance and return of Plethodontid salamanders to clearcut plots in the southern Blue Ridge Mountains. *Conservation Biology,* 11:983-989.

ASPRS LiDAR Committee. 2004. ASPRS Guidelines Vertical Accuracy Reporting for Lidar Data. edited by, LC Flood.

Baltsavias, E. P., 1999. Airborne laser scanning: basic relations and formulas.*ISPRS Journal of Photogrammetry and Remote Sensing*, *54*(2), 199-214.

Bater, C., Coops, N., Gergel, S., LeMay, V., and Collins, D., 2009. Estimation of standing dead tree class distributions in northwest coastal forests using LIDAR remote sensing. *Canadian Journal of Forest Research*, 39, 1080-1091.

Burton, T. M., and Likens G. E., 1975a. Salamander populations and biomass in the Hubbard Brook Experimental Forest, New Hampshire. *Copeia* 1975, 541–546.

Burton, T. M., and Likens, G. E., 1975b. Energy flow and nutrient cycling in salamander populations in the Hubbard Brook Experimental Forest, New Hampshire. *Ecology* 56, 1068–1080.

Carpenter, S. B., and Rumsey, R. L., 1976. Trees and Shrubs of Robinson Forest Breathitt County, Kentucky. *Castanea*, 41 (4), 277-282.

Cherry, M., 2006. *Hydrochemical characterization of ten headwater catchments in eastern Kentucky*. Thesis (Masters) Department of Forestry, University of Kentucky.

Carter, J., Schmid, K., Waters, K., Betzhold, L., Hadley, B., Mataosky, R., and Halleran, J., 2012. "Lidar 101: An Introduction to Lidar Technology, Data, and Applications." Revised. Charleston, SC: NOAA Coastal Services Center.

Charrier, R., and Li, Y., 2012. Assessing resolution and source effects of digital elevation models on automated floodplain delineation: A case study from the Camp Creek Watershed, Missouri. *Applied Geography*, 34, 38-46.

Childs, C., 2004. Interpolation surfaces in ArcGIS spatial analyst. ArcUser July–September, 32–35.

Clark, M. L., Clark, D. B., and Roberts, D. A., 2004. Small-footprint LiDAR estimation of sub-canopy elevation and tree height in a tropical rain forest landscape. *Remote Sensing of Environment*, 91(1), 68-89.

Collins, B., Kayen, R. E., 2006. Applicability of terrestrial LIDAR scanning for scientific studies in Grand Canyon National Park, Arizona. Reston, Va: U.S. Geological Survey.

Cupp Jr, P. V., 1980. Territoriality in the green salamander, Aneides aeneus. *Copeia*, 463-468.

Dalponte, M., Bruzzone, L., and Gianelle, D., 2011. A system for the estimation of single-tree stem diameter and volume using multireturn LIDAR data. *Geoscience and Remote Sensing*, IEEE Transactions on, 49(7), 2479-2490.

Davic, R. D., & Welsh Jr, H. H., 2004. On the ecological roles of salamanders. *Annual Review of Ecology, Evolution, and Systematics*, 405-434.

ESRI, 2014. ArcGIS Desktop: Release 10.1. Redlands, CA: Environmental Systems Research Institute.

Fleishman, E., MacNally, R., Fay, P., and Murphy, D. D., 2001. Modeling and predicting species occurrence using broad-scale environmental variables: an example with butterflies of the Great Basin. *Conservation Biology* 15, 1674-1685.

Flint, W. D., & Harris, R. N. (2005). The efficacy of visual encounter surveys for population monitoring of Plethodon punctatus (Caudata: Plethodontidae). Journal of Herpetology, 39(4), 578-584.

Flood, M., 2004. ASPRS guidelines. Vertical accuracy reporting for LiDAR data. http://www.asprs.org/society/divisions/ppd/standards/LiDAR%20guidelines.pdf [Accessed: 3rd May, 2015].

Farrell, D., 2012. LiDAR Initiative. Kentucky Transportations Cabinet.

Gifford, M. E., & Kozak, K. H., 2012. Islands in the sky or squeezed at the top? Ecological causes of elevation range limits in montane salamanders. *Ecography*, 35(3), 193-203.

Goerndt, M. E., Monleon, V. J., and Temesgen, H., 2011. A comparison of small-area estimation techniques to estimate selected stand attributes using LiDAR-derived auxiliary variables. *Canadian Journal of Forest Research*, 41(6), 1189-1201.

Gould, S. B., Glenn, N. F., Sankey, T. T., and McNamara, J. P., 2013. Influence of a dense, low-height shrub species on the accuracy of a LiDAR-derived DEM. *Photogrammetric Engineering and Remote Sensing,* 79 (5), 421-431.

Goulden, T., Jamieson, R., Hopkinson, C., and Sterling, S., 2014. Sensitivity of watershed attributes to spatial resolution and interpolation method of LIDAR DEMs in three distinct landscapes. *Water Resources Research*, 50, 3, 1908-1927

Grover, M. C., 2006. Comparative effectiveness of nighttime visual encounter surveys and cover object searches in detecting salamanders. *Herpetological Conservation and Biology*, 1(2), 93-99.

Hayes, R. A., 1998. Soil survey of Breathitt County, Kentucky. USDA-NRCS. U.S. Gov. Print. Office, Washington, DC.

Heurich, M., 2008. Automatic recognition and measurement of single trees based on data from airborne laser scanning over the richly structured natural forests of the Bavarian Forest National Park. *Forest Ecology and Management*, 255 (7), 2416–2433.

Hodgson, M. E., and Bresnahan, P., 2004. Accuracy of airborne LiDAR-derived elevation: Empirical assessment and error budget. *Photogrammetric Engineering and Remote Sensing*, 70(3), 331-339.

Hodgson, M. E., Jenson, J., Raber, G., Tullis, J., Davis, B. A., Thompson, G., and Schuckman, K., 2005. An evaluation of LiDAR-derived elevation and terrain slope in leaf-off condition. *Photogrammetric Engineering and Remote Sensing*, 62, 415-433.

Hyyppä, H., Yu, X., Hyyppä, J., Kaartinen, H., Kaasalainen, S., Honkavaara, E., and Rönnholm, P., 2005. Factors affecting the quality of DTM generation in forested areas. *International Archives of Photogrammetry, Remote Sensing and Spatial Information Sciences*, 36 (3/W19), 85-90.

Iverson, L. R., Dale, M. E., Scott, C. T., and Prasad, A., 1997. A gis-derived integrated moisture index to predict forest composition and productivity of ohio forests (U.S.A.). *Landscape Ecology*, 12(5), 331-348.

Kienzle, S., 2004. The Effect of DEM Raster Resolution on First Order, Second Order and Compound Terrain Derivatives. *Transactions in GIS*, 8 (1), 83-111.

Kim, S., 2008. "*Individual tree species identification using LIDAR-derived crown structures and intensity data".* PhD Dissertation, College of Forest Resources, University of Washington.

Koch, B., Heyder, U. and Weinacker, H., 2006. Detection of individual tree crowns in airborne LIDAR data. An approach to delineate tree crowns in mixed and deciduous temperate forests. *Photogrammetric Engineering and Remote Sensing*, 72, 357–363.

Kraus, K. and Pfeifer, N., 1998. Determination of terrain models in wooded areas with airborne laser scanner data. *ISPRS Journal of Photogrammetry and Remote Sensing* 53, 193–203.

Lee, H.S., 2004. A hybrid model for DTM generation from LiDAR signatures. PhD thesis, Department of Electrical and Computer Engineering, Mississippi State University.

Lefsky, M. A., Cohen, W. B., Parker, G.G., and Harding D. J., 2002. LIDAR remote sensing for ecosystem studies. *Bioscience* 52(1), 19-30.

Li, S., MacMillan, R. A., Lobb, D. A., McConkey, B. G., Moulin, A., and Fraser, W. R., 2011. LiDAR DEM error analyses and topographic depression identification in a hummocky landscape in the prairie region of Canada. *Geomorphology, 129,* 263-275.

Lim, S., Thatcher, C. A., Brock, J. C., Kimbrow, D. R., Danielson, J. J., and Reynolds, B. J., 2013. Accuracy assessment of a mobile terrestrial lidar survey at Padre Island National *Seashore. International Journal of Remote Sensing*, 34(18), 6355-6366

Lindsay, J. B., Rothwell, J. J., and Davies, H., 2008. Mapping outlet points used for watershed delineation onto DEM-derived stream networks. Water Resources Research, 44, 8.

Liu, X., 2008. Airborne LIDAR for DEM generation: Some critical issues. *Progress in Physical Geography*, 32, 1, 31-49.

MacKenzie, D. I., Nichols, J. D., Lachman, G. B., Droege, S., Royle J. A., and Langtimm C. A., 2002. Estimating site occupancy rates when detection probabilities are less than one. *Ecology* 83, 2248–2255.

Maerz, J. C., Nuzzo, V. A., and Blossey, B., 2009. Declines in Woodland Salamander Abundance Associated with Non-Native Earthworm and Plant Invasions. *Conservation Biology*, 23(4), 975-981.

Marvin, G. A., 1996. Life history and population characteristics of the salamander Plethodon kentucki with a review of Plethodon life histories. *American Midland Naturalist*, 385-400.

Marvin, G.A. 1998. Territorial behavior of the Plethodontid salamander Plethodon kentucki: Influence of habitat structure and population density. Oecologia 114:113–144.

MathWorks, T., 2004. Matlab. The MathWorks, Natick, MA.

Matsunaga, K., Nakaya, T., and Sugai, T., 2009. Simple DEM-Based Methods to Delineate Channel Networks for Hydrogeomorphological Mapping. *Transactions in GIS*, 13(1), 87-103.

Meng, X., Currit, N., and Zhao, K., 2010. Ground filtering algorithms for airborne LiDAR data: A review of critical issues. *Remote Sensing*, 2(3), 833-860.

Overstreet, J. C., 1984. *Robinson Forest inventory: 1980-1982.* University of Kentucky, College of Agriculture, Department of Forestry, Lexington, Kentucky, USA.

Peterman, W. E., and Semlitsch, R. D., 2014. Spatial variation in water loss predicts terrestrial salamander distribution and population dynamics. *Oecologia* 176(2), 357-369.

Peterman, W. E., & Semlitsch, R. D., 2013. Fine-scale habitat associations of a terrestrial salamander: the role of environmental gradients and implications for population dynamics. *Plos One,* 8, 5.

Petranka, J. W., 1998. Salamanders of the United States and Canada. Smithsonian Institution Press.

Petranka, J.W., 1999. Recovery of salamanders after clearcutting in the southern Appalachians: a critique of Ash's estimates. Conservation. Biology. 13(1): 203–205.

Petranka, J. W., Eldridge, M. E., & Haley, K. E., 1993. Effects of timber harvesting on southern Appalachian salamanders. *Conservation biology*, 363-370.

Popescu, S. C., 2007. Estimating biomass of individual pine trees using airborne LIDAR. *Biomass and Bioenergy*, 31(9), 646-655.

R Development Core Team, 2008. R: A language and environment for statistical computing. R Foundation for Statistical Computing, Vienna, Austria.

Rahman, M.Z., and Gorte, B.G.H., 2008. Individual tree detection based on densities of high points of high resolution airborne LIDAR. (conference paper.) University of Calgary, Canada.

Reutebuch, S.E., Andersen, H., and McGaughey, R.J., 2005 Light detection and ranging (LIDAR): an emerging tool for multiple resource inventory. *Journal of Forestry* 103(6), 286-292.

Reutebuch, Stephen E., et al., 2003. Accuracy of a high-resolution LiDAR terrain model under a conifer forest canopy. *Canadian Journal of Remote Sensing.* 29(5), 527-535.

Royle, J. A., 2004. N-mixture models for estimating population size from spatially replicated counts. Biometrics 60:108–115.

Royle, J. A., Nichols, J. D., and Kery, M., 2005. Modelling occurrence and abundance of species when detection is imperfect. *Oikos* 110, 353–359.

Ruszkiczay-Rüdiger, Z., Fodor, L., Horváth, E., and Telbisz, T., 2009. Discrimination of fluvial, eolian and neotectonic features in a low hilly landscape: A DEM-based morphotectonic analysis in the Central Pannonian Basin, Hungary. *Geomorphology*, 104(3), 203-217.

Sangster, C., 2002. Validating LIDAR – evaluating LIDAR accuracy using GPS. Lawrencetown, Nova Scotia: Applied Geomatics Research Group, Centre of Geographic Science

Santitamnont P., and Miphokasap, P., 2013. Extraction of Mangrove Biophysical Parameters Using Airborne LIDAR. Multidisciplinary Digital Publishing Institute.

Schneider, D.R., 2010. "*Salamander communities inhabiting ephemeral streams in a mixed mesophytic forest of southern Appalachia*". Thesis, Indiana University of Pennsylvania, Indiana, Pennsylvania, USA.

Semlitsch, R.D. 1980. Geographic and local variation in population parameters of the slimy salamander Plethodon glutinosus. *Herpetologica* 36:6–16.

Setiyoko, A., Kumar, A. 2012. Comparison analysis of interpolation techniques for DEM generation using Cartosat-1 stereo data. *International Journal of Remote Sensing and Earth Sciences,* 9(2):78-87

Sithole, G., 2001. Filtering of laser altimetry data using a slope adaptive filter. International *Archives of Photogrammetry, Remote Sensing and Spatial Information Sciences* 34, 3/W4, 203–10.

Smalley, G.W., 1986. Classification and evaluation of forest sites on the Northern Cumberland Plateau. USDA-FSS,O-60, Southern Forest Research Station, New Orleans, LA. 76.

Spaete, L. P., Glenn, N. F., Derryberry, D. R., Sankey, T. T., Mitchell, J. J., and Hardegree, S. P., 2011. Vegetation and slope effects on accuracy of a LiDAR-derived DEM in the sagebrush steppe. *Remote Sensing Letters*, *2*(4), 317-326.

Srinivasan, S., Popescu, S. C., Eriksson, M., Sheridan, R. D., and Ku, N. W., 2014. Multi-temporal terrestrial laser scanning for modeling tree biomass change. *Forest Ecology and Management*, 318, 304-317.

Stauffer, D. F., 2002. Linking populations and habitats: Where have we been? Where are we going? Pages 53-61 in J. M. Scott, P. J. Heglund, M. L. Morrison, J. B. Haufler, M. G. Raphael, W. A. Wall, and F. B. Samson, editors. Predicting species occurrences: issues of scale and accuracy. Island, Washington, D.C., USA.

Stereńczak, K., and Kozak, J., 2011. Evaluation of digital terrain models generated in forest conditions from airborne laser scanning data acquired in two seasons. *Scandinavian Journal of Forest Research,* 26 (4), 374-384.

Stoker, J., et al., 2007. Report of the First National LiDAR Initiative Meeting, USGS Land Remote Sensing Program, Reston, Va.

Su, J., and Bork, E., 2006. Influence of vegetation, slope, and LiDAR sampling angle on DEM accuracy. *Photogrammetric Engineering and Remote Sensing*, 72(11), 1265-1274.

Symonds, M. R., and Moussalli, A., 2011. A brief guide to model selection, multimodel inference and model averaging in behavioral ecology using Akaike's information criterion. Behavioral Ecology and Sociobiology, 65(1), 13-21.

Terrasolid Ltd., 2012. TerraScan User's Guide. URL: http://www.terrasolid.com/download/tscan.pdf, last accessed 10th May 2015.

Thurow, G.R. 1976. Aggression and competition in eastern Plethodon (Amphibia, Urodela, Plethodontidae). *Journal of Herpetology,* 10, 277–291.

Vogeler, J. C., Hudak, A. T., Vierling, L. A., and Vierling, K. T., 2013. LIDAR-Derived Canopy Architecture Predicts Brown Creeper Occupancy of Two Western Coniferous Forests. *The Condor*, 115(3), 614-622.

Vosselman, G., 2000. Slope based filtering of laser altimetry data. International Archives of Photogrammetry. *Remote Sensing and Spatial Information Sciences*, 33(B3/2), 935-34

Wannasiri, W., Nagai M., Honda K., Santitamnont P., and Miphokasap, P., 2013. Extraction of Mangrove Biophysical Parameters Using Airborne LIDAR. Multidisciplinary Digital Publishing Institute. *5*(4), 1787-1808.

Welsh, H. H., and Droege, S., 2001. A Case for Using Plethodontid Salamanders for Monitoring Biodiversity and Ecosystem Integrity of North American Forests. *Conservation Biology*, 15(3) 558-569.

Wenger, S. J., 2007. Tutorial for Running Zero-Inflated Abundance Models Accounting for Incomplete Detection in R. Ecological Society of America, http://www.esapubs.org/archive/ecol/E089/166/ZIA_R_Tutorial.pdf

Wenger, S. J., and Freeman, M. C., 2008. Estimating species occurrence, abundance, and detection probability using zero-inflated distributions. *Ecology*, 89(10), 2953-2959.

Wyman, R. L., and Jancola, J., 1992. Degree and scale of terrestrial acidification and amphibian community structure. *Journal of Herpetology*, 392-401.

Wyman, R. L., 1998. Experimental assessment of salamanders as predators of detrital food webs: effects on invertebrates, decomposition and the carbon cycle. *Biodiversity and Conservati*on 7, 641–650.

Yang, P., Ames, D. P., Fonseca, A., Anderson, D., Shrestha, R., Glenn, N. F., and Cao, Y., 2014. What is the effect of LIDAR-derived DEM resolution on large-scale watershed model results?. Environmental Modelling and Software, 58, 48-57.

VITA

NAME	Wesley A. Staats	
EDUCATION	B.S. in Forestry University of Kentucky	
PROFFESSIONAL POSITIONS	Teachers assistant University of Kentucky	August 2013- May 2014, August 2014- May 2015
	Research assistant University of Kentucky	August 2013- August 2015
	Parks intern Louisville Metro Parks	May 2013- August 2013
	Veg management intern US Forest Service	May 2012 - March 2013
	Natural areas restoration Louisville Metro Parks	June 2011 - August 2011